4-2020

Storm-Dominated Diatomite: Transport and Deposition From Micro-Texture

Taylor Kelln

LOMA LINDA UNIVERSITY
School of Medicine
in conjunction with the
Faculty of Graduate Studies

_____

Storm-Dominated Diatomite: Transport and Deposition From Micro-Texture

by

Taylor Kelln

_____

A Thesis submitted in partial satisfaction of
the requirements for the degree
Master of Science in Geology

_____

April 2020

Each person whose signature appears below certifies that this thesis in his/her opinion is adequate, in scope and quality, as a thesis for the degree Master of Science.

_____, Chairperson

Kevin E. Nick, Associate Professor of Geology

_____

V. Leroy Leggitt, Professor of Geology

_____

Gina Roque-Torres, Assistant Professor of Radiology

ACKNOWLEDGEMENTS

I would like to thank Dr. Kevin Nick for his unwavering support of this research and of myself. It was his belief that brought this work to fruition.

I would also like to thank the committee as well as Loma Linda University's School of Dentistry for facilitating the use of their micro-CT instruments and their progressive application of this technology to the geosciences.

Lastly, I would like to thank my father who continually spurred my interest in the sciences and continues to do so until this day. And I would like to thank my mother, who I'm told was an inspiring biologist to all in her life, both in and outside the laboratory.

CONTENT

FIGURES

Figure Page

TABLES

Tables Page

ABBREVIATIONS

SEM	Scanning Electron Microscope
Micro-CT	Micro-Computed Tomography
WESGF	Wave-Enhanced Sediment-Gravity Flow

ABSTRACT OF THE THESIS

Storm-Dominated Diatomite: Transport and Deposition From Micro-Texture

by

Taylor Kelln

Master of Science, Graduate Program in Geology
Loma Linda University, March 2020
Dr. Kevin Nick, Chairperson

Unusually thick accumulations of diatomite and diatomaceous mud- and siltstones occur throughout the Mio-Pliocene along the Pacific margin. These extensive micro-fossil assemblages represent an important biostratigraphic resource, record of environmental conditions, and are economically relevant as unconventional reservoirs, sources and seals. Most depositional models for diatomaceous sediments tend to emphasize diatom productivity sufficient to overcome siliciclastic dilution and reflect a low-energy depositional regime with passive settling of diatoms through the water column. However, the diatomaceous sediments of the Pisco Basin, Peru, have been observed in longitudinally bedded, wavy, non-parallel laminated deposits, interpreted as hummocky-swaley cross-stratification. Other outcrop observations include tempestite-like sequence stacking, normal grading, and syndepositional soft-sediment deformation, suggesting a bedload orgin for the Pisco diatomite under a combined-flow regime and storm-like conditions. Such diatomite can also be found associated with fossil marine vertebrate burial.

This study sought to investigate these findings at the level of micro-texture though thin section imaging, SEMs of freshly parted rock surfaces, and micro-CT modeling. Notable textures observed include graded micro-couplets containing a normally graded

silt component and reverse graded diatomaceous component, predominantly observed in hummocky-swaley cross-stratified diatomite and swale drapings. In a stacked channel complex of interlaminated diatomite-siltstone, wave-enhanced sediment gravity flows were found as a graded triplet capped in purest diatomite. These suggest a bedload origin for much of the Pisco's diatomaceous sediments, and mirror textures previously derived in mudstone flume experiments, further suggesting that diatoms may entrain, flocculate, and accumulate in a manner effectively similar to clays. These findings also call into question the diatomite necessarily reflects a low-energy to passive depositional regime. Likewise, with respect to the Pisco Basin, it remains probable that much of its fossil content encased in diatomaceous sediments met their fate under a tractional regime rather than due to the slow-settling of diatoms and their components.

CHAPTER ONE

INTRODUCTION

This thesis illustrates that diatomite and similar fine-grained diatomaceous sediments can accumulate during current-dominated depositional regimes, namely under combined-flow and storm-like conditions. This conclusion stands in contrast to previous assumptions that emphasize a hemipelagic origin where diatomaceous sediments are the product of the slow and low-energy settling of diatoms from the water column. Tractional diatomite was found to form significant sequences in the Pisco Basin, interpreted as storm-derived due to tempestite-like sequence stacking and the presence of hummocky-swaley cross-stratification whose lamination was found to be a composite of graded micro-couplets. Sediment-gravity flow textures are also detailed, further suggesting a bedload origin for the Pisco diatomite.

Chapter 1 reviews depositional models for mudstone and diatomite, and their importance within the Pisco Basin. The conditions leading up to combined flow are also reviewed, alongside any resultant stratification, bedforms, and tempestite sequence stacking. Tractional mudstone textures are also reviewed, many of which are mirrored in the Pisco diatomite. In Chapter 2, a paper prepared for publication is presented, detailing the methods, results, and conclusions of this research. Lastly, a depositional and textural atlas for the diatomaceous sediments of the Pisco comprises Chapter 3, including any samples previously unpublished in Chapter 2.

On Diatomite, Mudstones, and the Pisco Formation

Mudstones are the most abundant sedimentary rock type, both comprising and recording the bulk of geologic history, yet comparatively, they remain much more poorly understood than their coarser counterparts. Despite this, they remain important in the influence of groundwater flow, act as hydrocarbon sources, reservoirs, and seals, as well as acting as recorders of pelagic and benthic biogenic production and organic matter burial. They are often easily weathered and appear homogenous to the casual observer due to their fine grain size with most grains smaller than 62 μm. Though their sedimentary structures are frequently subtle and difficult to resolve, mudstones can host a wide variety of sedimentary structures and may potentially accumulate under much more active depositional regimes and settings than previously realized (Schieber et al., 2007; Schieber and Southard, 2009; Bohacs et al., 2014; Lazar et al., 2015; Yawar and Schieber 2017).

Muds and mudstones were once thought to only readily accumulate under quiet, low-energy conditions, mainly in deeper water, only to be intermittently distributed by weaker currents (Potter et al., 2005; Schieber and Southard 2009). Diatomite, a bioclastic mudstone composed almost entirely of the siliceous remains of diatoms, is no exception. However, nearly a decade's worth of textural studies and flume experiments on clay and silt deposition have slowly begun to erode this view (e.g. Schieber, 2007; Schieber and Southard, 2009; Yawar, 2017). While it is now largely accepted that muds may readily deposit under similar tractional regimes that deposit sand and other coarser material, a tractional genesis for diatomite and diatomaceous mudstones remains comparatively understudied. This absence is surprising given diatomite's high abundance during the Neogene around the Pacific margin, specifically during the middle Miocene to lowermost

Pliocene, typified by the Onnagawa and Funakawa formations of Japan as well as the oil-rich and highly productive Monterey Shale of California (Ingle, 1981; Slatt, 2011).

Another diatomaceous formation is the Pisco Formation of Peru, a lagerstätte bearing a wealth of vertebrate fossils, and many large, well-preserved, and articulated marine vertebrates are found preserved in diatomaceous sediments (Brand, 2004; Esperante, 2015). High nutrient supply linked to coastal upwelling in the eastern equatorial Pacific has been previously invoked as a mechanism leading to the high diatom productivity seen in the region (Kemp and Baldauf, 1993; Brand, 2004; Esperante, 2015). More recently, signs of reworked diatomite and diatomaceous mud- and siltstones have been recognized by several studies, sometimes associated with fossil marine vertebrate burial (e.g. Flemming, 2014; Stanton, 2014), and one of the more peculiar sedimentary structures observed is that of hummocky-swaley cross-stratified diatomite. These wavy and gently truncating structures are thought to result from combined-flow in the onshore-offshore transition (Dumas and Arnott, 2006). They typically form in silt to fine sand during waning storm conditions (Dott and Bourgeois, 1982). Recognition of these structures expands the potential depositional regimes and environments in which diatomite may accumulate and places its deposition far closer to shore than previously realized.

On Tempestites and Combined-Flow Regimes

Tempestites define a broad range of event beds thought to reflect storm deposits. Variable stacking sequences can be found within tempestite beds (e.g. Myrow et al., 2002; their Figure 1), though most are recognized by a basal, scoured surface, sometimes with an accompanying lag, and overlying deposits reflecting storm conditions. These can include combined-flow bedforms such as hummocky-swaley cross-stratification (Dumas and Arnott, 2006) to wave-modified gravity-flows, as well as the oscillatory and unidirectional current endmembers, wave- and current-ripples respectively (Myrow, 2002). The idealized hummocky sequence originally proposed by Dott and Bourgeois (1982, their Figures 3, 5) provides an excellent conceptual model of storm-induced stacking patterns, including the muddy and bioturbated tops formed during subsequent fair-weather conditions. These are summarized in Figure 1, including the idealized hummocky sequence, common variations, and amalgamated sequences produced from successive and frequent storm events. However, internal stratification within tempestites is often far more complex and variable, reflecting a constantly changing intersection between wave oscillations, geostrophic currents, and density-induced flow present during a storm regime (Myrow and Southard, 1996; their Figure 7).

The forces which generate combined-flow in a shallow marine setting are wind-driven coastal set-up, a pressure gradient formed by the storm waves incident with the coast, and the resulting, bottom-hugging relaxation flow that evolves to geostrophic flow as it deflects with the Coriolis force (and overview of these forces can be seen in Dalrymple and James, 2010, their Figure 6, p. 171). Thus, storm waves comprised the oscillatory component of combined-flow and work to generate the bottom-hugging, unidirectional component of flow (Dalrymple and James, 2010). However, wave-

turbulence can also entrain and suspend sediment-laden currents, intermittently driven offshore during storms as wave-modified turbidites and hyperpycnal flows. These form a third variable to a combined-flow regime during storms and can equally influence resulting bedforms in addition to the causes listed above (Myrow, 2002).

Dumas and Arnott (2006) conducted flume experiments on two different sediments of size 0.11 and 0.17 mm and demonstrated the progressive variations in preserved bedforms during waning, combined-flow conditions. Under lower, net-aggradation rates (1 mm/min), concave-up swaley bedforms are preferentially preserved, while at higher net-aggradation rates (4.2 mm/min), concave-down, hummocky bedforms are preferentially preserved (Dumas and Arnott, 2006, their Figure 3). They propose that higher on the shoreface, swaley cross-stratification will persist over hummocky. In that subenvironment, conditions lead to lower net aggradation rates and higher sediment transport rates due to proximity to coastal set-up. Hummocky structures will be preserved further offshore where net aggradation rates are apparently higher (Dumas and Arnott, 2006, their Figure 4). Thus, the ratio of hummocky to swaley bedforms can further refine the particular position of deposition within the onshore-offshore transition zone. An overview of storm processes, currents, and resultant bedforms can be seen in Figure 2 alongside the expected stratification of wave-modified turbidity currents across the shelf environment.

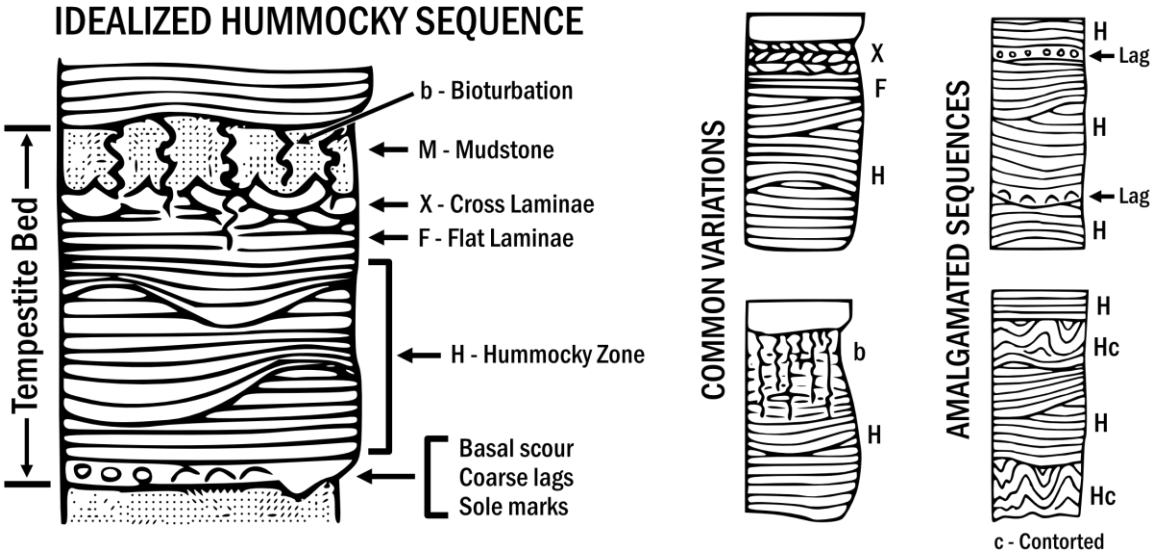

Figure 1. The idealized hummocky sequence comprising a tempestite deposit after Dott and Bourgeois (1982). Basal scour, soles marks, and lags mark storm onset. The hummocky zone marks deposition during waning storm conditions during a combined flow regime. Flat laminae and cross laminae are formed at the very end of a storm, resulting from the lingering effects of bottom-hugging geostrophic currents which may persist well after a storm subsides due to coastal setup. A mudstone draping caps the sequence, marking post-storm settling of fines. Sequence may show varying degrees and depths of bioturbation. Tempestites may be truncated by successive storm events and the deposition of overlying tempestites, and can show considerable variation depending on lithology and the exact nature of a storm. If storms are frequent enough, certain parts of the sequence can be completely lost or overwritten, resulting in amalgamated sequences.

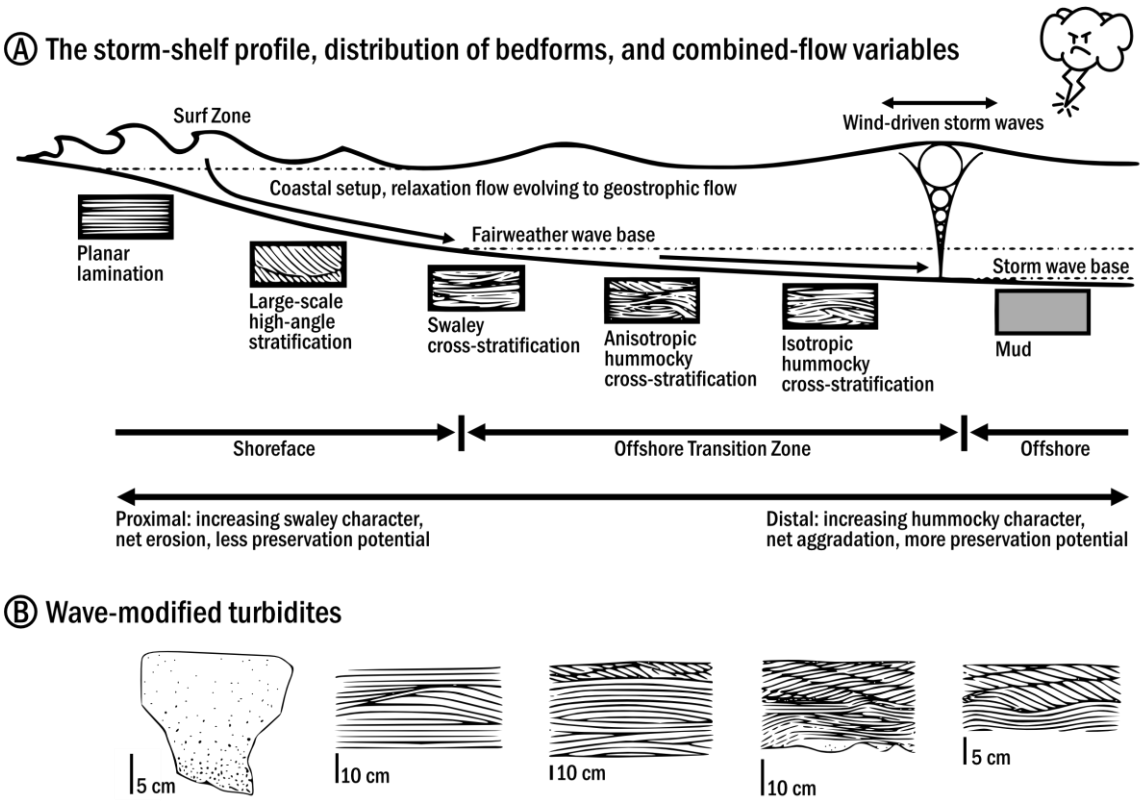

Figure 2. The storm-shelf profile (A) with predictive stratification modified from Dumas and Arnott (2006) and wave-modified turbidites (B), a type of tempestite, and their distribution along the shelf modified from Myrow et al. (2002). The offshore transition zone is thought to reflect the primary sub-environment of storm deposition by way of hummocky-swaley cross-stratification, with increasing swaley character toward the shore and increasing hummocky character toward the offshore. These deposits reflect combined flow which results from the interplay between amped-up storm waves and bottom hugging currents evolved from coastal setup. Storm-entrained turbidites can also be deposited under combined flow and exhibit fabrics such as hummocky-swaley cross-stratification and combined flow ripples in addition to conventional turbidite-like grading and Bouma sequencing.

On Tractional Mudstone Textures from Flume Experiments

Flume experiments on mudstones have yielded a variety of diagnostic, depositional textures which reveal their tractional genesis. Siliclastic mudstones have been shown to accrete as migrating ripples under unidirectional flow, where floccule prone muds develop low-angle foresets (Schieber, 2007; Schieber and Southard, 2009; Schieber and Yawar, 2009). These bear the same asymmetrical profile as a unidirectional current ripple and are created as sediment is transported over the stoss side in the form of diverging boundary-layer streaks. These streaks act as point sources at the ripple brink and feed avalanches of floccule-rich sediment lobes down the lee slide of ripples (Schieber and Southard, 2009, their Figures 1, 4). The highly fluidized nature of these floccule ripples (80-90% water by volume) leaves them highly susceptible to post-depositional compaction, often overwriting signs of flocculation, flattening original cross-lamination, and producing planar-parallel fabrics (Schieber, 2007; Schieber and Southard, 2009; Schieber and Yawar, 2009).

Likewise, Yawar and Schieber (2017) illustrated that coarse silt can segregate from clays during bedload transport. A thin veneer of silt is left behind by migrating floccule ripples which, in time, can form laminated deposits of couplets where relatively coarser silt is sequestered in laminae and lenses that are overlain by clay floccules with finer silt suspended within its matrix (Yawar and Schieber, 2017, their Figure 19). Pre-compaction clays were shown to exhibit randomly oriented, cardhouse fabrics. Coarse silt sequestrations can either exist as continuous laminae or discontinuous as lenses depending on sediment supply, where higher supply produces laminations, and lower supply produces lenses (Yawar and Schieber, 22017, their Figure 23). A proposed model for the formation of couplets can be seen in their Figure 22, where. Migrating floccules of

clay containing both coarse and fine silt inclusions collide. These collisions preferentially liberate coarse silt, causing it to drop out and form what is essentially a lag—a sequestered lens or lamina of coarse silt. Floccules continues to migrate, still containing the fine silt component, and deposit over coarser silt sequestrations. This forms couplets that can show sharp to moderate normal grading among silt grains, fining upward into clays. With continued ripple migration, several generations of these couplets can be deposited overlying one another (Yawar and Schieber, 2017). An summary of bedforms and textures dervived from these flume experients can be seen in Figure 3, including Yawar and Schiebers' (2017) model on the generation of coarse silt sequestrations.

General conclusions of these experiments posit that flow properties and fluid dynamics are more important than the material they may entrain (Schieber and Yawar, 2009). Similar, tractional textures have been observed by this study in the Pisco diatomite, only furthering this assertion. It remains entirely possible that similar processes of bedload migration and flocculation occurred in the Pisco Basin but in a diatomaceous rather than purely siliciclastic substrate. It is important to note, however, that while diatoms do form floccules and aggregates, they do not coalesce as a result of electro-statics as seen in clays. Instead, the aggregate as a result of collision, affected by water column turbulence, and diatom stickiness, affected by extracellular polymeric substances (Thornton, 2002). Both colonial and mat-forming species also occur naturally 'flocculated' as a result of interlocking spines, processes, and interwoven frustules.

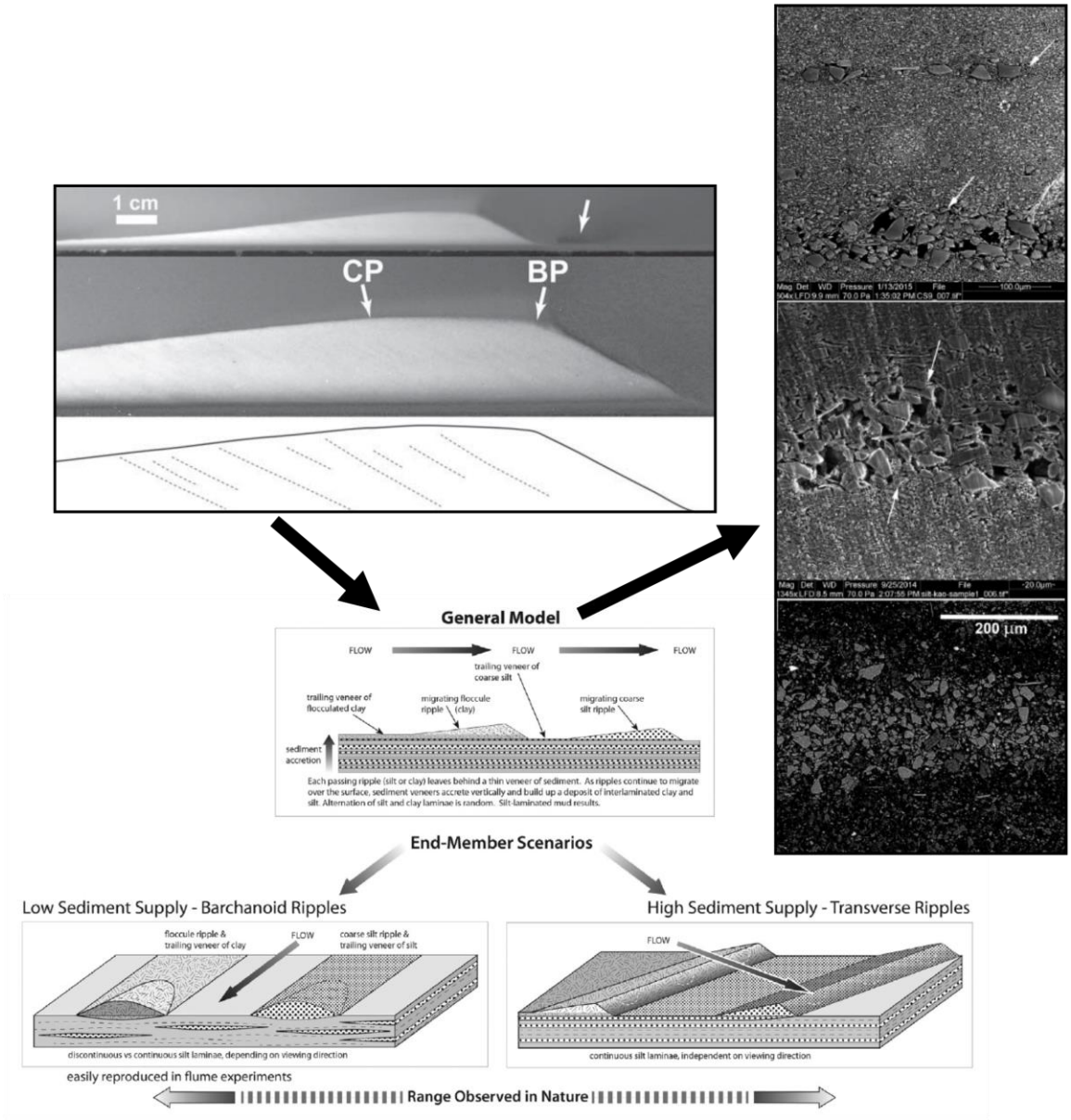

Figure 3. Migrating floccule ripple that remained at attached to flume wall in experiments conducted by Scheiber and Southard (2009, top image). Note scoured pit at arrow in addition to the ripple's crest point (CP), brinkpoint (BP), and faint internal cross-lamination. The lower image shows a conceptual model on the formation of interlaminated silt and muds from Yawar and Schieber (2017). In their model, colliding floccules preferentially liberate coarse silt which builds up in lamina or lenses, depending on sediment supply, and initiates ripple formation. The left-most image shows SEMs of resin stabilized flume textures, where coarse silt can be seen sequestered as laminae at and between the white arrows.

References

Bohacs, K. M., Lazar, O. R., & Demko, T. M. (2014). Parasequence types in shelfal mudstone strata—Quantitative observations of lithofacies and stacking patterns, and conceptual link to modern depositional regimes. Geology, 42(2), 131-134.

Brand, L. R., Esperante, R., Chadwick, A. V., Porras, O. P., & Alomía, M. (2004). Fossil whale preservation implies high diatom accumulation rate in the Miocene–Pliocene Pisco Formation of Peru. Geology, 32(2), 165-168.

Dalrymple, R. W., & James, N. P. (Eds.). (2010). Facies models 4. Geological Association of Canada.

Dott Jr, R. H., & Bourgeois, J. (1982). Hummocky stratification: significance of its variable bedding sequences. Geological Society of America Bulletin, 93(8), 663-680.

Dumas, S., & Arnott, R. W. C. (2006). Origin of hummocky and swaley cross-stratification—The controlling influence of unidirectional current strength and aggradation rate. Geology, 34(12), 1073-1076.

Esperante, R., Brand, L. R., Chadwick, A. V., & Poma, O. (2015). Taphonomy and paleoenvironmental conditions of deposition of fossil whales in the diatomaceous sediments of the Miocene/Pliocene Pisco Formation, southern Peru—A new fossil-lagerstätte. Palaeogeography, Palaeoclimatology, Palaeoecology, 417, 337-370.

Fleming, M. A. (2014). Sedimentology of Marine Vertebrate Burial in the Miocene Pisco Fm., Peru (Master's thesis) Loma Linda University, Loma Linda, CA.

Ingle Jr, J. C. (1981). Origin, Depositional History, and Correlation of Miocene Diatomites Around North Pacific Margin. AAPG Bulletin, 65(5), 940-940.

Kemp, A. E., & Baldauf, J. G. (1993). Vast Neogene laminated diatom mat deposits from the eastern equatorial Pacific Ocean. Nature, 362(6416), 141-144.

Lazar, O. R., Bohacs, K. M., Schieber, J., Macquaker, J. H., & Demko, T. M. (2015). Mudstone Primer: Lithofacies variations, diagnostic criteria, and sedimentologic-stratigraphic implications at lamina to bedset scales. SEPM (Society for Sedimentary Geology).

Myrow, P. M., & Southard, J. B. (1996). Tempestite deposition. Journal of Sedimentary Research, 66(5), 875-887.

Myrow, P. M., Fischer, W., & Goodge, J. W. (2002). Wave-modified turbidites: combined-flow shoreline and shelf deposits, Cambrian, Antarctica. Journal of Sedimentary research, 72(5), 641-656.

Potter, P. E., Maynard, J. B., & Depetris, P. J. (2005). Mud and mudstones: Introduction and overview. Springer Science & Business Media.

Schieber, J., Southard, J., & Thaisen, K. (2007). Accretion of mudstone beds from migrating floccule ripples. Science, 318(5857), 1760-1763.

Schieber, J., & Southard, J. B. (2009). Bedload transport of mud by floccule ripples—Direct observation of ripple migration processes and their implications. Geology, 37(6), 483-486.

Schieber, J., & Yawar, Z. (2009). A new twist on mud deposition: mud ripples in experiment and rock record. The sedimentary record, 7(2), 4-8.

Slatt, R. (2011). Important geological properties of unconventional resource shales. Open Geosciences, 3(4), 435-448.

Stanton, C. (2014). Correlation and Paleoenvironments above West T9. 3 Tuff, Pisco Formation, Peru (Master's thesis). Loma Linda University, Loma Linda, CA.

Thornton, D. C. (2002). Diatom aggregation in the sea: mechanisms and ecological implications. European Journal of Phycology, 37(2), 149-161.

Yawar, Z., & Schieber, J. (2017). On the origin of silt laminae in laminated shales. Sedimentary Geology, 360, 22-34.

CHAPTER TWO

STORM-DOMINATED DIATOMITE:

TRANSPORT AND DEPOSITION FROM MICRO-TEXTURE

Abstract

Unusually thick accumulations of diatomite and diatomaceous mud- and siltstones occur throughout the Mio-Pliocene along the Pacific margin. These extensive micro-fossil assemblages represent an important biostratigraphic resource, record of environmental conditions, and are economically relevant as unconventional reservoirs, sources and seals. Most depositional models for diatomaceous sediments tend to emphasize diatom productivity sufficient to overcome siliciclastic dilution and reflect a low-energy depositional regime with passive settling of diatoms through the water column. However, the diatomaceous sediments of the Pisco Basin, Peru, have been observed in longitudinally bedded, wavy, non-parallel laminated deposits, interpreted as hummocky-swaley cross-stratification. Other outcrop observations include tempestite-like sequence stacking, normal grading, and syndepositional soft-sediment deformation, suggesting a bedload orgin for the Pisco diatomite under a combined-flow regime and storm-like conditions. Such diatomite can also be found associated with fossil marine vertebrate burial.

This study sought to investigate these findings at the level of micro-texture though thin section imaging, SEMs of freshly parted rock surfaces, and micro-CT modeling. Notable textures observed include graded micro-couplets containing a normally graded silt component and reverse graded diatomaceous component, sometimes capped in purest diatomite. These were typically found to comprise the laminae of hummocky-swaley deposits, sometimes gently truncating one another. Couplets showing more gradual

grading are interpreted as the product of wave-entrained sediment-gravity flows in the offshore transition zone, while more sharply graded couplets are interpreted as the product of floccule ripple migration. Triplet architectures were also observed within a stacked channel complex containing interlaminated diatomite-siltstone, interpreted as successive wave-enhanced sediment gravity flows that drove scour, channel migration, and rapid in-fill. Current ripple profiles were also found preserved within an early diagenetic and diatomaceous zeolite, where diatoms and other platy grains were found to conform to foreset architecture.

Textures observed are markedly similar to those produced in mudstone flume experiments and suggest that diatoms may flocculate, migrate, and deposit in a manner effectively similar to clay-silt mixtures. These textures call into question the notion that diatomaceous sediments necessarily reflect a low-energy depositional regime and call for caution when assigning biostratigraphic horizons and environmental interpretations to possibly reworked assemblages. Degrees of reworking may also affect diatomite's economic potential, meriting further investigation. With respect to the Pisco Basin, it remains possible that much of its fossil content encased in diatomaceous sediments met their fate under a tractional regime rather than due to the slow settling of diatoms and their components.

Introduction

Unusually thick accumulations of shallow marine diatomite and diatomaceous mudstones occur around the Pacific margin during the Miocene-Pliocene (Ingle, 1981). The Pisco Formation is one of these, bearing a lithology rich in diatoms, volcanic ash, and fine terrigenous silt often found alongside well-preserved and often articulated fossil marine vertebrates, several of which have been the basis of paleontological studies. The relatively excellent preservation and articulation of vertebrates within this fossil lagerstätte have been attributed to the diatomaceous sediments of the Pisco, but both the manner and rate of diatom deposition leading to preservation have been subjects of debate (Brand et al., 2004; Gariboldi et al., 2017).

Apparent storm-derived sedimentary structures hosted in diatomite and diatomaceous siltstones have been previously observed in outcrop (Flemming, 2014; Stanton, 2014). This study examines these and other reworked successions of diatomaceous sediments, to characterize their texture and micro-texture, and to more accurately infer the processes and environmental conditions associated with their accumulation. Observations suggest a tractional genesis for much of the Pisco's diatomaceous sediments, with textures mirroring those derived via flume experiment on muddy lithologies (e.g., Schieber et al., 2007; Schieber and Southard, 2009; Schieber and Yawar, 2009; Lazar et al., 2015; Yawar and Schieber, 2017). This further suggests that diatoms may entrain, flocculate, sort, and accumulate in a manner effectively similar to clays as seen in migrating floccule ripples and wave-enhanced sediment-gravity flows. Additionally, outcrop-scale stratification reflects an influence of combined-flow, differential scour and fill, tempestite-like sequence stacking, and apparent deposition above storm-wave-base (Dott and Bourgeois, 1982; Dumas and Arnott, 2006).

Future challenges include quantifying exact processes of flow and accumulation through flume experiments on diatoms and the effect lateral transport has on the preservation potential and taphonomy of diatoms. Reworked assemblages of diatoms may also exhibit unique physical properties compared to non-reworked assemblages as a result of their exhumation and increased exposure to abrasion and fragmentation. This may affect a deposit's porosity and permeability, as well as its reservoir, source, or seal potential. This work also suggests pairing textural observations with biostratigraphy before assigning horizons to plausibly reworked, and therefore time-averaged, diatom assemblages. These implications are perhaps most salient to the diatomaceous, Micocene analogues of the Pisco Formation about the Pacific Margin.

Geologic Setting

The tectonism along the Peruvian margin was primarily controlled by the oblique subduction of the Nazca/Farallon Plate under the South American Plate beginning in the Cretaceous (Di Celma, 2017; Pilger, 1981; Thornburg and Kulm, 1981). By the Late Cretaceous through Eocene, the complex of igneous rocks comprising the Andean Coastal Batholith began emplacement to become the Cordillera of Peru (Cobbing, 1999) along which eight forearc basins rest, one of which is the Pisco Basin. The Pisco Basin is bisected into West and East Pisco segments by a prominent structural ridge known as the Outer Shelf High composed of Precambrian and Paleozoic metasediments and other crystalline rocks. The High runs subparallel to the Andean Coastal Batholith with the Cenozoic sediments of both West and East Pisco onlapping it (Thornburg and Kulm, 1981). The West Pisco Basin formed a seaward slope basin and its counterpart, the East Pisco Basin, our area of study, form a shallow but deeply inset and semi-protected

embayment sandwiched between the Outer Shelf High and the Andean Coastal Batholith (Dunbar et al., 1990; de Muizon and DeVries, 1985). The eventual subaerial exposure of the East Pisco Basin was facilitated by the subduction of the Nazca Ridge beginning in the middle Miocene and continuing until today (Pilger, 1981). Figure 1 shows a map overview of East Pisco and related structural features.

The Pisco Formation within East Pisco Basin is comprised of sediments ranging from the middle Miocene through Pliocene recording at least three major transgressive cycles, vertically progressing from coarse bioclastic conglomerates and sandstones grading upward into siltstones, mudstones. Biogenic deposits, including the diatomite and diatomaceous mudstones of this study, are most abundant at the top (Dunbar, 1990). These fining upward sequences (P0, P1, and P2) are unconformity-bounded by three, widespread erosional surfaces (PE0.0, PE0.1, and PE0.2) and progressively onlap to merge as a composite, basal unconformity marking the lower boundary of the Pisco Formation (informally PE0) to the southwest and northeast. Figure 2 presents a schematic, dip-oriented stratigraphic diagram of the Pisco Formation after DiCelma et al. (2017), which summarizes these features.

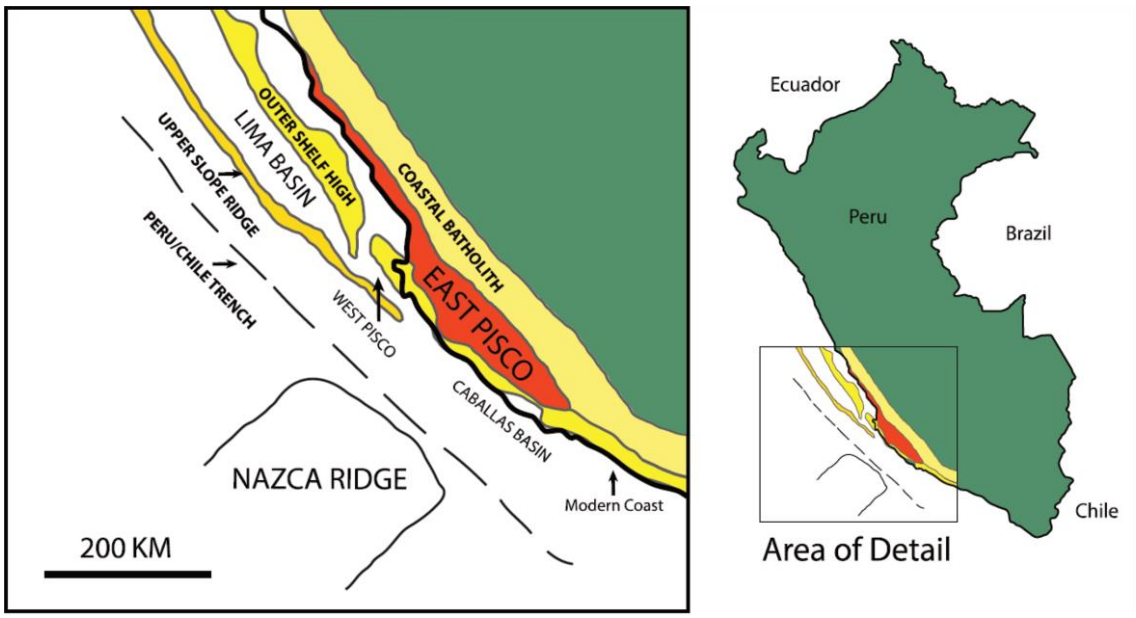

Figure 1. Overview of basins and structural features surrounding East Pisco Basin (orange), the study area. Map modified from Flemming (2014), based on Dunbar et al. (1990), which was based on Travis et al. (1976) and Thornburg and Klum (1981).

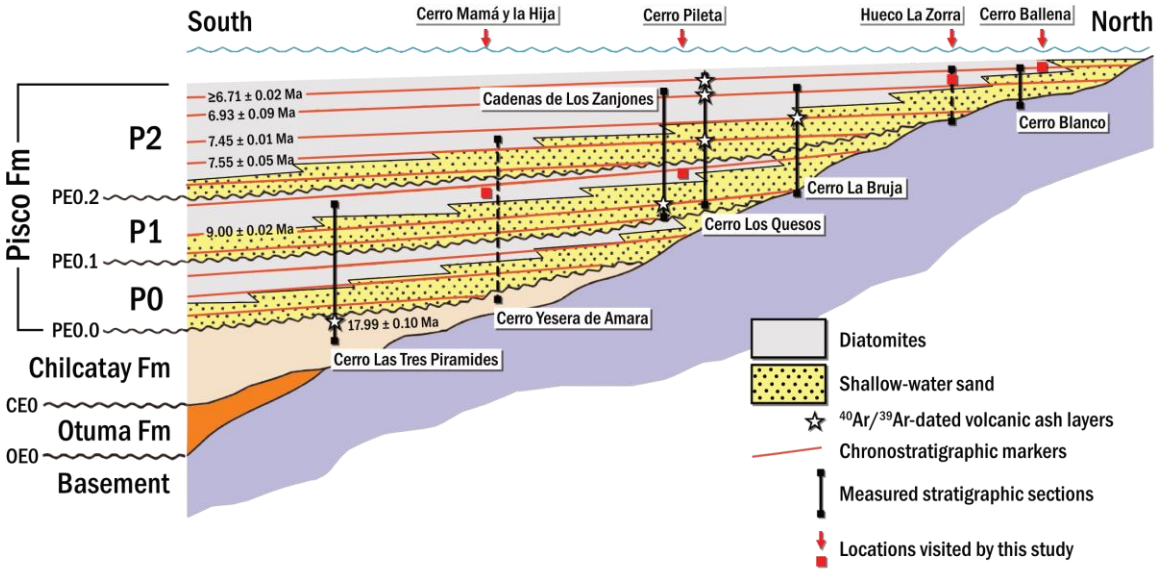

Figure 2. Schematic, dip-oriented stratigraphic diagram for the Pisco Formation (not to scale) after DiCelma et al. (2017), showing the position of the stratigraphic sections on which the diagram is based (vertical black lines) and supplemented by a cursory stratigraphic examination of two additional sites (vertical dashed lines). The locations visted by this study have been drawn over the original diagram (red boxes, red arrows), showing approximate outcrop and sampling locations with respect to the greater Pisco Formation.

Field Sampling and Laboratory Methods

The East Pisco Basin was visited with the intent of identifying diatomite and diatomaceous mudstones that exhibited either structure or stratification indicative of reworking. The basin was explored at large, with three locations yielding exceptional samples to be examined in detail in this study. An overview of the locations and their coordinates can be seen in Figure 3. At each location, lithology was documented, and oriented samples were collected directly from the outcrop. At Cerro Hueco la Zorra, a section was logged. Other sections were logged on previous visits.

Laboratory work began by preparing oriented samples for thin sections, SEM surfaces, and micro-CT blocks after methods derived from O'Brien and Slatt (1990). Oriented blocks were cut from outcrop samples for thin section preparation with SEM and micro-CT samples cut and extracted from the paired excess of the thin section sample block. In the case of SEM samples, where possible, smaller samples were cored from the paired block with a coring drill bit measuring 1 cm in diameter. For more friable samples, a jeweler's saw was used to carefully cut out smaller pieces. Before stub mounting, a narrow band was carved about the sample's circumference/body before snapping the sample in two, creating two freshly-parted surfaces fractured cleanly across the sample width, one of which was then stub mounted. Samples were prepared with views looking both perpendicular to and into lamination. Samples were imaged in a Tescan Vega LSII scanning electron microscope.

Micro-CT samples were initially prepared by coating their exterior with low viscosity epoxy before microtoming off a slice ~1.5 mm thick to reveal a core of pure rock surrounded and stabilized by an epoxy shell. Later, for less friable samples, small blocks of rock were extracted with a jeweler's saw and sanded down to even smaller

blocks ~5 mm thick using P400 sandpaper by hand. Samples were scanned in a Bruker SkyScan 1272 micro-CT scanner at 5 μm and 1 μm resolutions depending on the sample. Model rendering, voxel reconstruction, and quantitative measurements were conducted using Bruker's 3D Suite of software including DataViewer (for orthographic projections), CTAn (for quantitative analysis), and CTVox (for model reconstruction and presentation). Table 1 details specific scan parameters and thresholding by sample.

The results are divided into observations and interpretations, which are further divided by locality.

Table 1. Micro-CT scanning parameters by sample. Resultant resolution is higher than the resolution set before scanning.

Sample	Voxel resolution	Filter	Rotation Step	Frame Averaging	Reconstruction Angular Range	Source Voltage	Source Current
CHZ-1	3 μm	Al 0.25 mm	0.2°	4	192.80°	50 kV	200 μA
CP-4	6 μm	Al 0.25 mm	0.2°	3	192.40°	50 kV	200 μA
CMH	6 μm	None	0.2°	4	192.80°	50 kV	200 μA

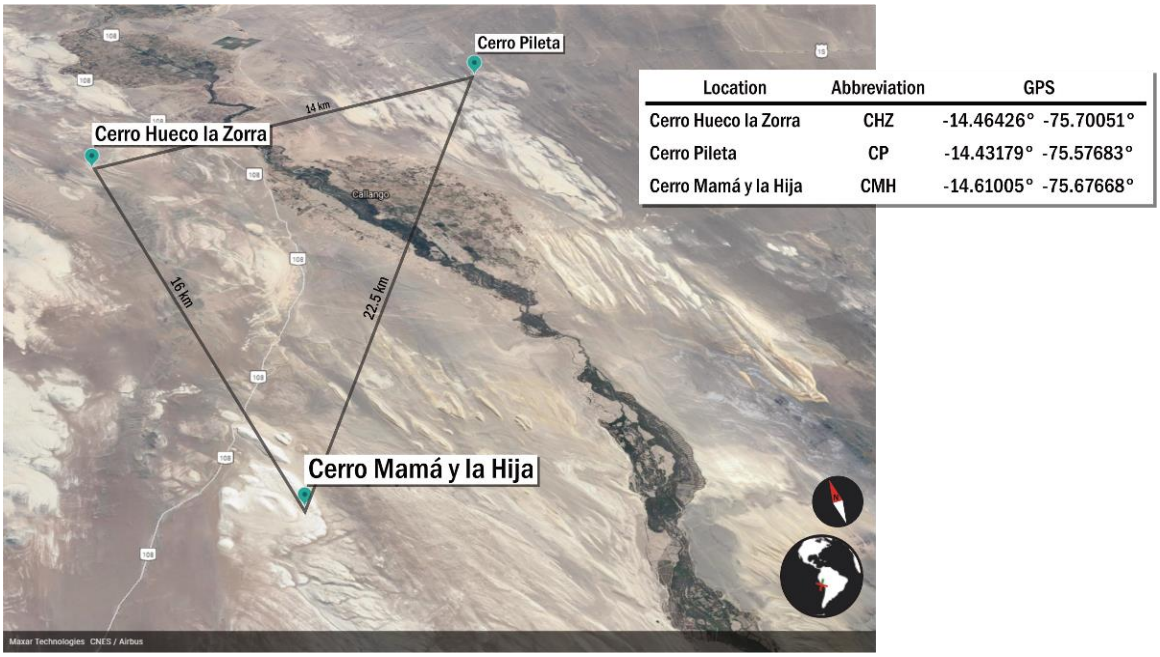

Figure 3. Oblique aerial of East Pisco and the three locations visited by this study from Google Earth. Outcrop exposures of the Pisco Formation can be visually approximated by the extent of the bright white hills below, often diatomaceous, tuffaceous, and fossiliferous. The Ica River crosscuts the image. Map data: Google, Maxar Technologies, CNES/Airbus. Camera altitude: 13,337m. Camera location: -14.66229, 75.60221.

Observations

Location 1: Cerro Hueco la Zorra: Cross Laminated Diatomite

The measured section at Cerro Hueco la Zorra (Figure 4) is primarily composed of diatomaceous to tuffaceous siltstone with several exceptionally diatomaceous intervals. The majority of the outcrop exhibited discontinuous, wavy, non-parallel lamination alongside thinner beds of more continuous, planar laminated lithologies. Lamination within diatomite was often faint and sometimes mistaken as purely parallel, continuous, and planar in the field, though upon careful inspection in the lab and reinspection of outcrop images, gentle truncation could often be discerned (e.g. Figure 4B). In siltier lithologies, hummocky-swaley cross-stratification was a more distinct, notable and frequent (Figure 4C). Sometimes isolated swales and scour structures could be seen with diatomite drapings at their bases and as infill. Coprolites are common, many phosphatized, and in the case of sample CHZ-2, were sometimes found to preserve pristine examples of articulated diatoms (Figure 4D). These provide a good comparison to fragmented and compacted diatoms found to compose many of the samples. An overview of the constituent grains of Cerro Hueco la Zorra's diatomite can be found in Figure 5, illustrating the variety of conditions in which diatoms are found to be preserved as well as the detrital and volcaniclastic grains found amongst them. Diatom frustules tend to eclipse and obscure one another, making observations difficult for the fist-time observer compared to more common lithologies hosting discrete grain boundaries. Thus, Figure 5 is also intended as a quick orientation to diatomite in thin section and SEM.

The most notable sample from this locality was cross-laminated diatomite (CHZ-1), where platy grains such as diatoms, biotite, and ash define internal micro-laminae and foreset architecture (Figure 6). Of particular note are two laminae containing distinctly

downlapping micro-foresets showing migration toward the right (Figure 6B, C). These are interrupted by two laminae containing wavy, non-parallel, and largely discontinuous micro-laminae, some of which show plausible onlap. The preservation of cross-lamination may be a result of early cementation as the sample is markedly less-friable than other. While the diatomaceous content shows little signs of alternation, a blocky cement cursory analysis suggests in a zeolite can be seen both surrounding and growing within the frustules seen in Figure 5C, D.

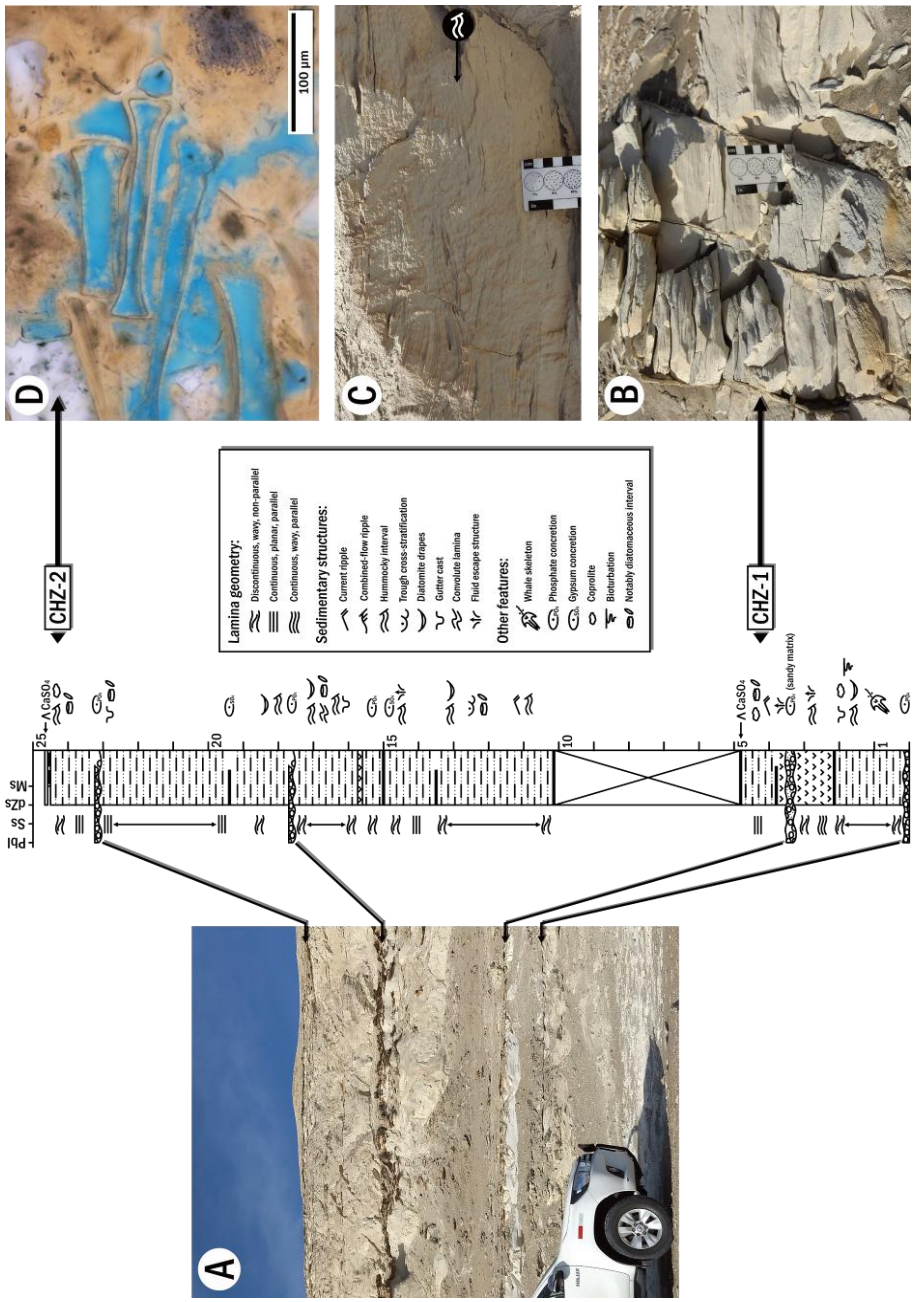

Figure 4. Outcrop view of Cerro Hueco la Zorra (A) and corresponding geologic section. Most of the section is composed of siltstone, diatomaceous siltstone, and diatomite in varying purities, though it is difficult to discern the difference between each in the field before lab analysis. Resistant layers are phosphate-pebble conglomerates. (B) shows diatomite in outcrop, interpreted initially as planar laminated by later revealed to contain a current rippled micro-texture. (C) shows the typical outcrop view of diatomaceous siltstone, often exhibiting discontinuous, non-parallel, wavy lamination, interpreted in this instance as hummocky cross-stratification. Very faint signs of truncation can be discerned in outcrop upon careful inspection. (D) shows phosphatized diatoms within a coprolite, showing near-pristine examples of diatoms in cross-section, the constituents of much of the Pisco.

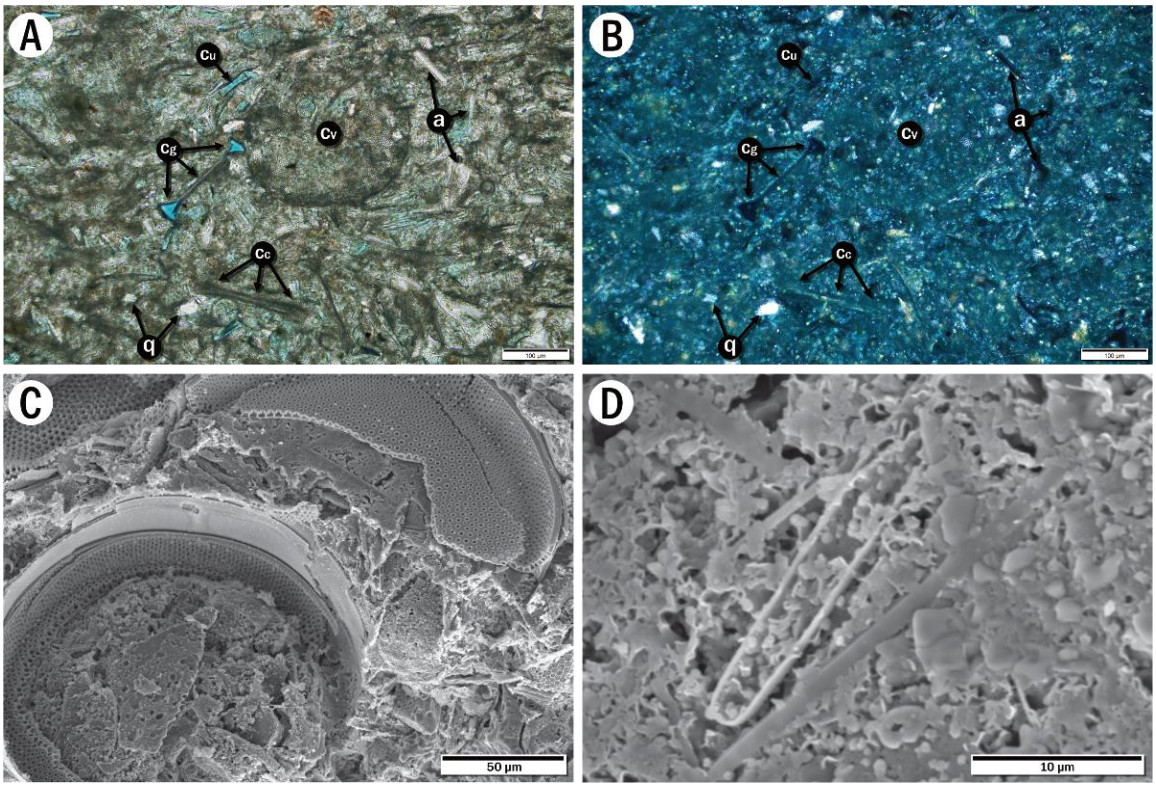

Figure 5. Overview of sample CHZ-1 and its diatomaceous content in thin section (A) and with polarizers crossed (B). 'Cv' rests at the center of a centric diatom in valve view and 'Cg' a centric diatom in girdle view, often exhibiting a double-hairpin-like appearance as articulated girdle bands tend to resist compaction. 'Cu' notes an uncompacted centric, highly porous, while 'Cc' notes a fully compacted centric--platy and not to be confused with mica minerals which also persist in the sample. Minor constituents include smaller quartz, 'q,' and feldspars, as well as ash 'a.' Both (C) and (D) are SEM images showing that, while diatoms remain largely unaltered, the sample appears to be well-cemented in a diagenetic zeolite, likely originating from the partial alteration of the volcanic component of the rock. Note mineral growth in and upon frustules. SEMs taken at 10kV.

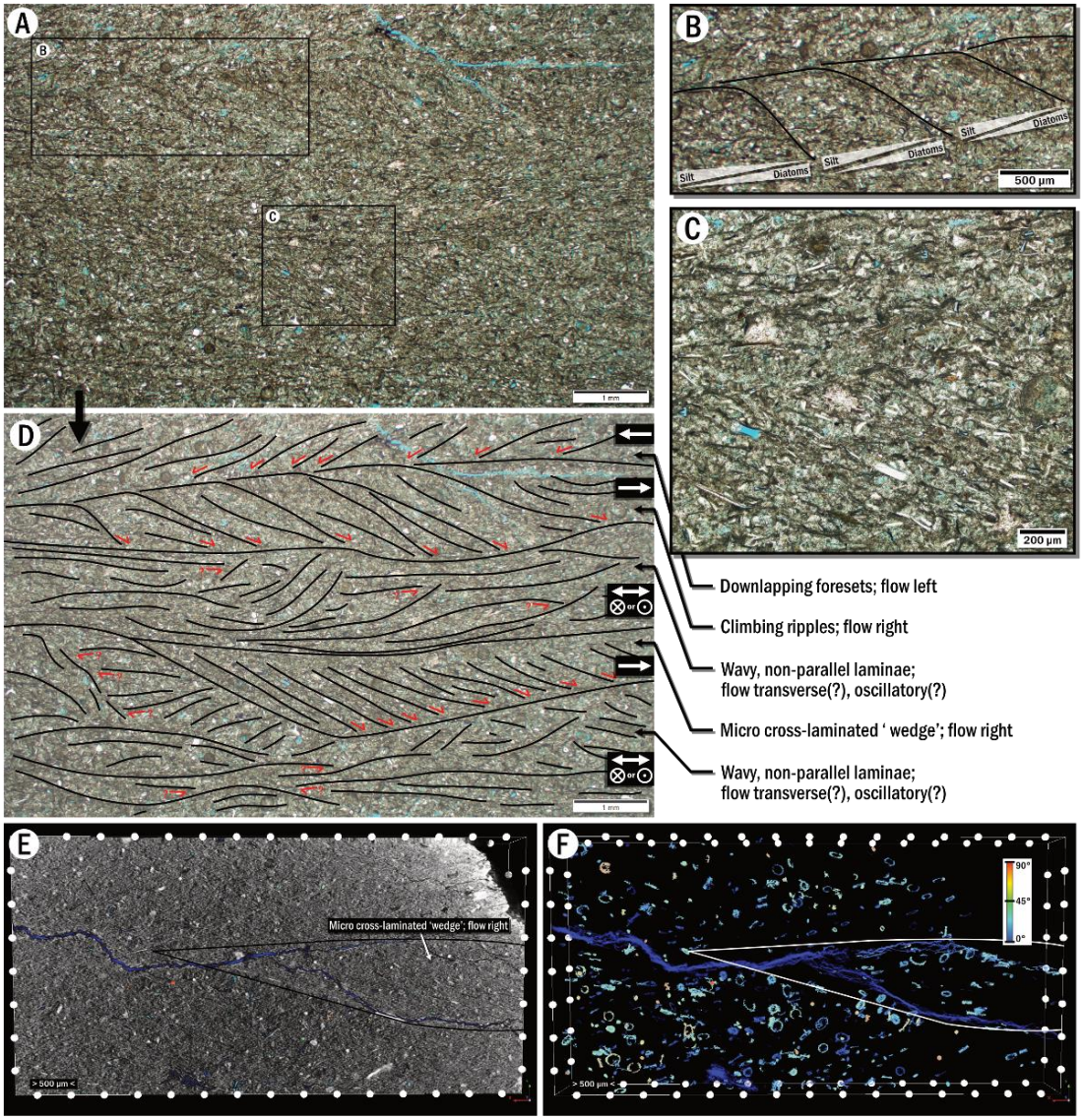

Figure 6. Sample CHZ-1, cross-laminated diatomite as seen in thin section (A-D) and micro-CT model (E, F). (A) shows the unmarked thin section. (B) is a magnification of climbing ripples showing internal sorting, normally graded in silt with crests and foresets capped in diatoms. (C) is another magnification showing the micro-foresets of a downlapping 'wedge' where platy grains such as centric diatoms, biotite, and ash can be seen conforming to foreset architecture. It is overlain by wavy micro-laminae. (D) is a line drawing over (A), divided into five, approximately mm thick macro-laminae with bulk flow direction and interpretations labeled to the right. (E) is a rock surface micro-CT model of the paired block used to create (A). The same micro cross-laminated 'wedge' is outlined for comparison. In (F), the rock has been subtracted, and large, centric diatoms have been isolated by the porous rings about their resistant girdle bands. Rings have been color-coded for orientation to show dip direction. The ghostly blue line across the image is an artificial crack, a good visual marker between (E) and (F). Preservation of micro-cross-laminae is attributed to early zeolite diagenesis. Scan taken at 1 µm resolution. All pores were thresholded from the background and gradual despeckling was conducted until centric ring pores were isolated.

Location 2: Cerro Pileta: Storm-dominated Diatomite

Diatomite is abundant at the Cerro Pileta locality, bearing wavy, non-parallel lamination that varies from moderately continuous to discontinuous. Scour features are common, including swales and their associated drapings, gutter casts, and one case of trough cross-stratification containing a sandy basal lag. Aggradational structures such as hummocks are also common. In exceptional cases, some larger swales host fossil whale bones at their base that are draped by diatomite. As with much of the Pisco Formation, these whale skeletons are articulated and well-preserved, previously attributed to the rapid accumulation of the diatomaceous sediments, which encase them (Flemming, 2014). Figure 7 shows a whale rostrum protruding from outcrop at the base of an exaggerated swale that conforms with a laterally traceable and extensive bounding surface that appears to truncate a previous deposit. The lithology both above and below the surface is composed of diatomite to diatomaceous siltstone. Soft-sediment deformation is frequently encountered, resulting in the convolution and subsidence of local laminae, sometimes traceable across significant successions of laminae, apparently as a result of fluid migration.

The diatomite of Cerro Pileta is friable, poorly cemented (if at all), and its diatomaceous component is diagenetically unaltered. However, across samples, a micro-matrix of diatomaceous debris is pervasive (Figure 8), a composite of disarticulated spines, processes, and frustule fragments. Large, well-articulated centric diatoms are most discernable, many compacted horizontally (Figure 8; 10). Parallel-aligned pennate ‘bundles’ were present within the matrix of several samples (Figure 8). Large, porous mat fragments were found suspended with the laminae of a hummocky-swaley cross-stratified

sample, and internally, the mat is a composite patchwork of similar parallel-aligned pennate ‘bundles’ (Figure 9).

Laminae from swale drapings and hummocky-swaley samples were normally graded in samples containing relatively coarser silt, which forms a basal sequestration, lamina, or lens, and fines upward into diatomite and finer-silt. These graded couplets can range in scale from nearly bedded (Figure 10B) to micro-laminated (Figure 10C). Couplets can be gently dipping, pinching out, and possibly truncating one another (Figure 11B). Silt sequestrations survive soft-sediment deformation in micro-CT views, and while left dipping and contorted, couplet architecture was largely preserved (Figure 11C).

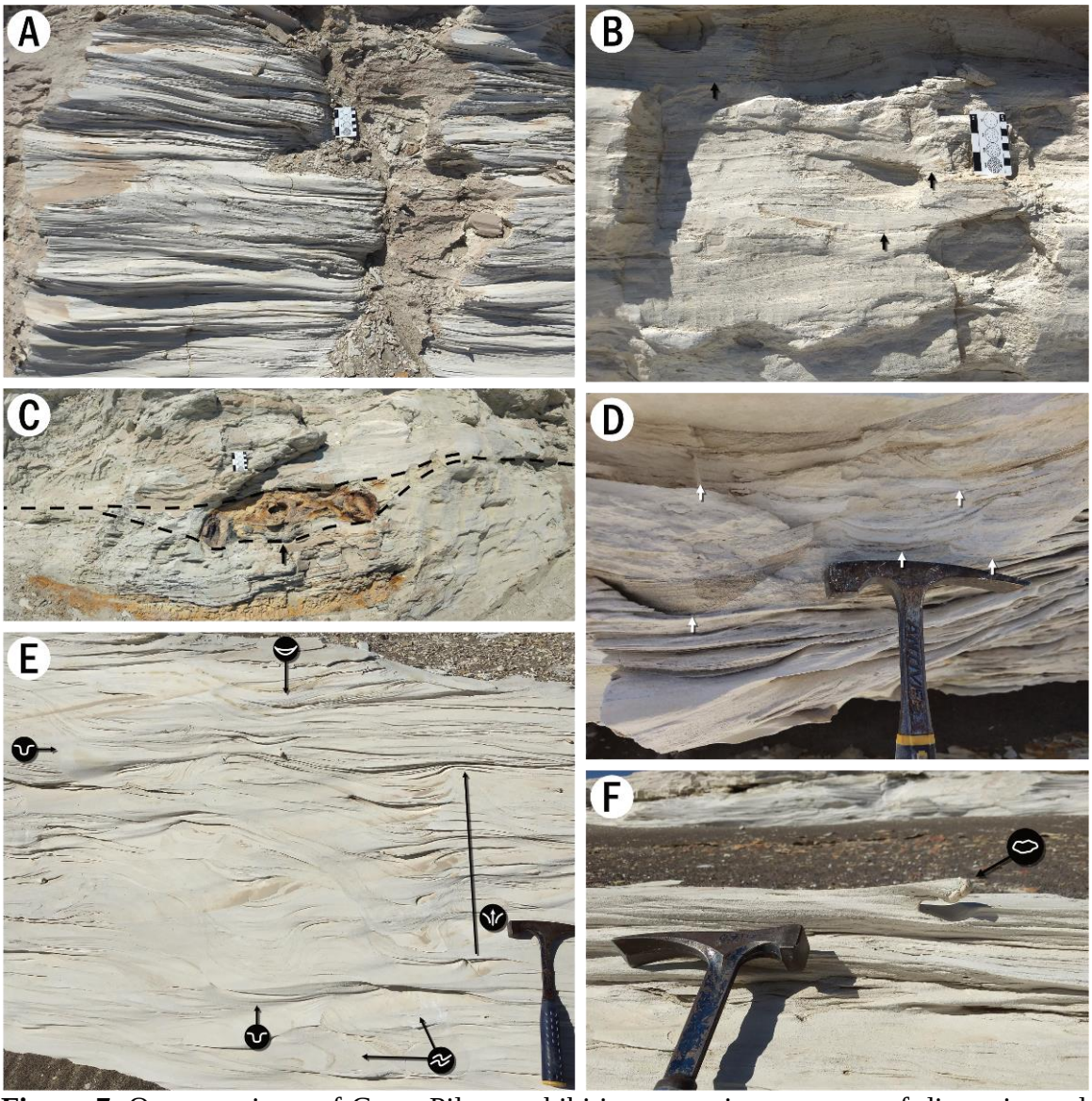

Figure 7. Outcrop views of Cerro Pileta, exhibiting extensive outcrops of diatomite and diatomaceous siltstones bearing wavy, non-parallel, and moderately continuous to discontinuous lamination. Lithology is often tuffaceous as well. (A) is interpreted as low-angle, amalgamated hummocky-swaley cross-stratification. Exaggerated swales can often be found within successions (B; black arrows point to swale bases), and in exceptional cases, even contain fossil marine vertebrates (C; a whale rostrum in cross-section). A trough cross-stratified interval can be seen in (D; white arrows at base of troughs), the left-most one exhibiting a sandy lag at the base. (E) shows a gently dipping exposure with several features: extensive soft-sediment deformation attributed to fluid escape, deformed to convolute laminae, as well as sharply eroded gutter casts and more gently dipping swale drapes. A precarious coprolite can be seen in (F, white arrow), exhumed by recent aeolian erosion.

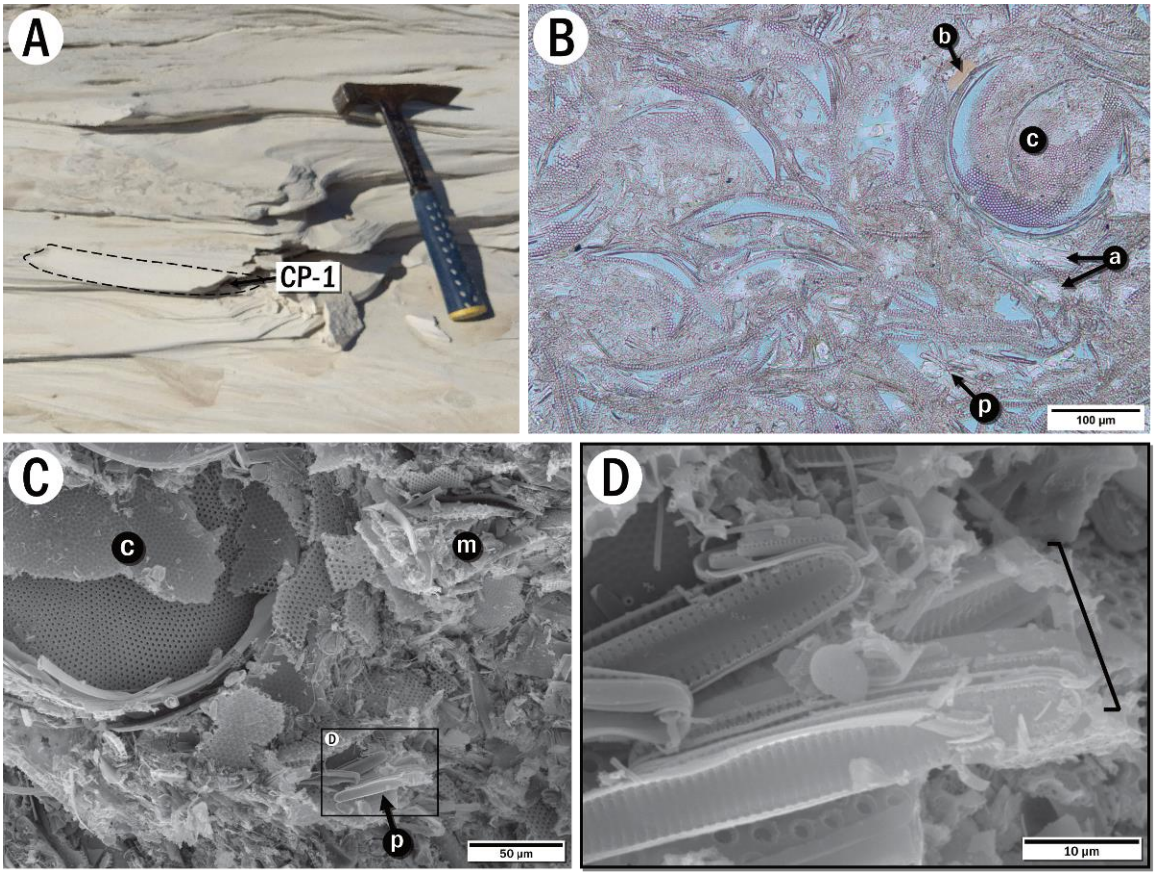

Figure 8. Overview of sample CP-1, a notably pure tongue of diatomite. (A) shows the sample in outcrop. (B) shows the sample in thin section, and offers an excellent overview of the diatomaceous content at Cerro Pileta in general. A large centric diatom in valve view can be seen at 'c', and small bundles of pennates at 'p'. Other constituents include ash 'a' and biotite 'b' as the diatomite found at this locality is largely tuffaceous as well as diatomaceous. Rock tends to be poorly cemented and highly fissile to friable. (C) shows an SEM of a freshly parted rock surface. In addition to a few articulated individuals, much of the matrix 'm' of the sample is largely diatom hash, a mix of frustule fragments, spines, and resting spores. Note the parallel-aligned 'bundle' of pennate diatoms magnified in (D), interpreted here as colony liberated from larger mat fragments. For comparison, see the larger mat fragment of Figure 9 (sample CP-2).

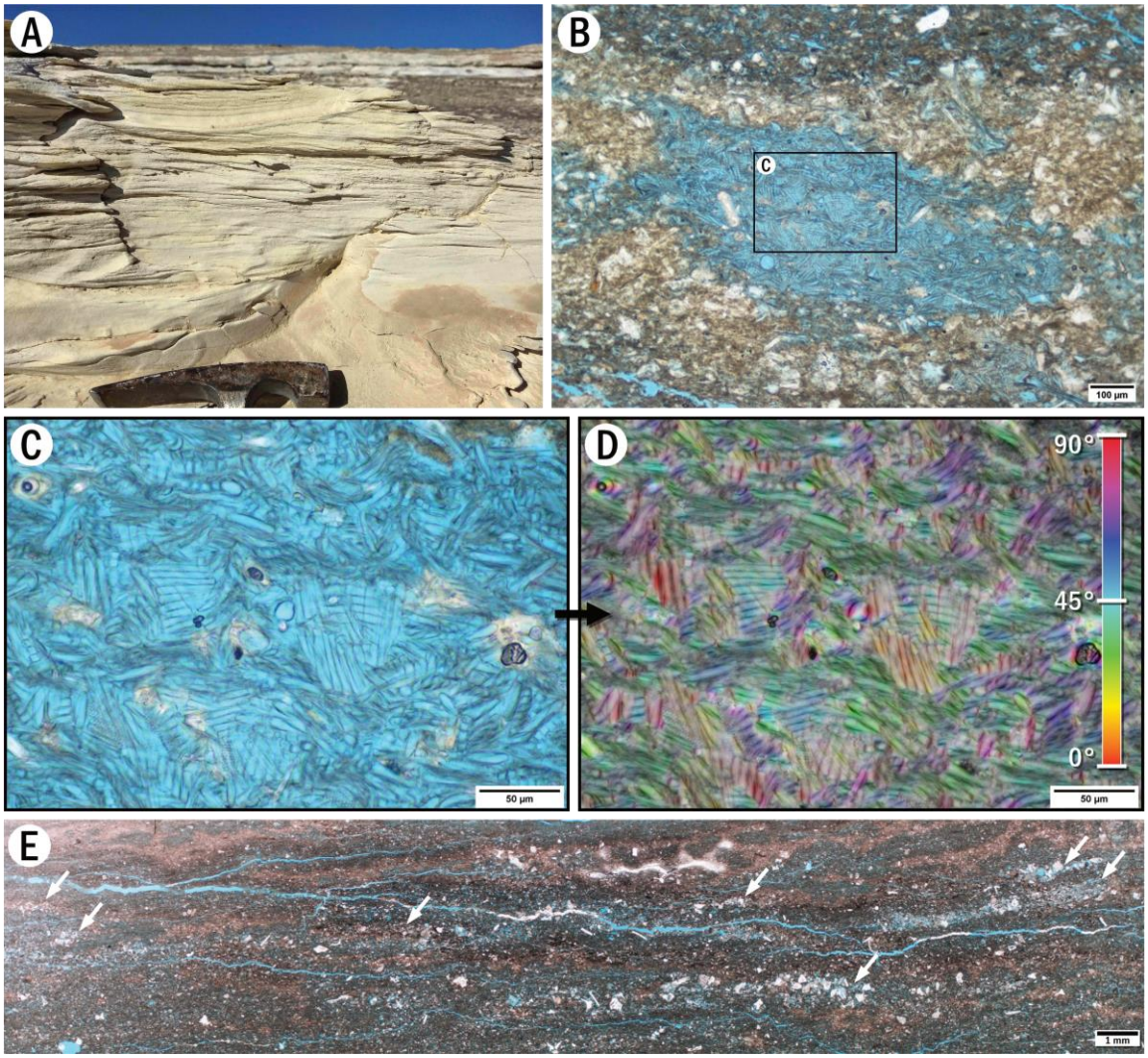

Figure 9. Overview of sample CP-2, distinct hummocky-swaley cross-stratified diatomite. (A) shows the sample in outcrop. (B) shows it in thin section, where several porous specks could be spotted in the matrix. A closer look (C) reveals these are pennate diatom aggregates, interpreted as mat fragments. In (D), OrientationJ, and ImageJ plug-in (Püspöki et al. 2016), has been used to color-code diatom orientation, reaveal in the aggregate as a patchwork of parallel-aligned, pennate 'bundles. Similar bundles of pennates can be observed within the matrix of other samples across Cerro Pileta (see Figure 8; sample CP-1), suggesting differential aggregate break-up due to lateral transport. The sample also shows silt sequestrations by way of lenses (E, white arrows), a texture that suggests the tandem migration of silt and diatomaceous floccule ripples.

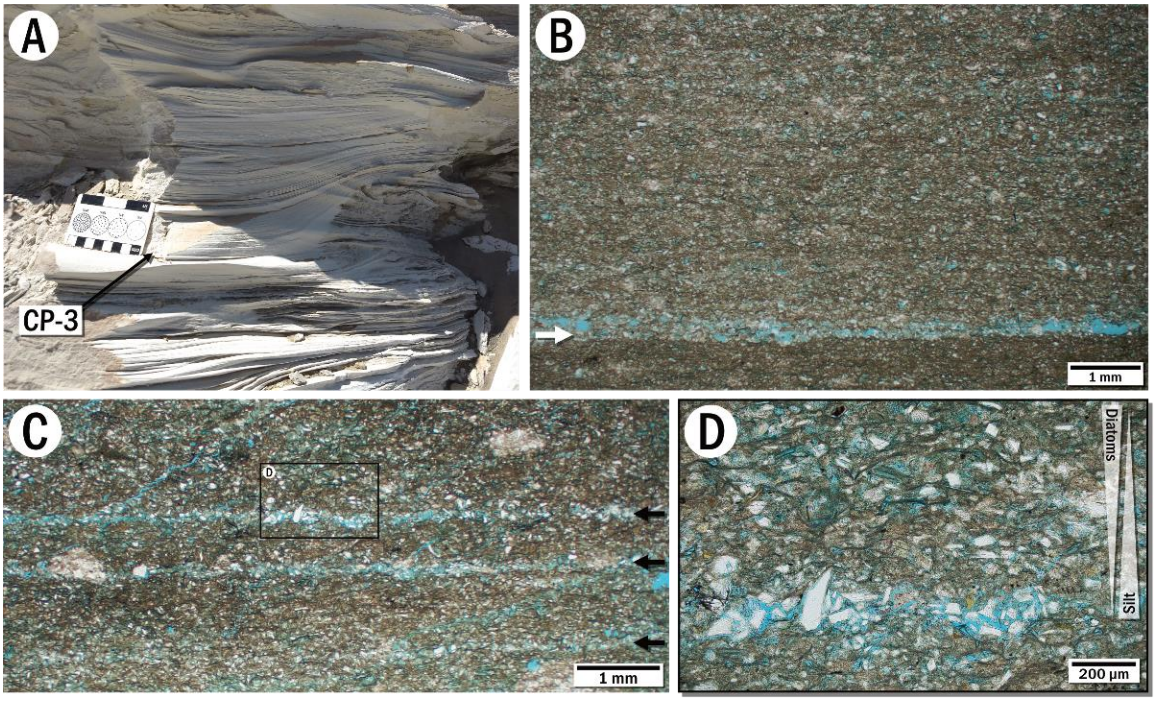

Figure 10. Overview of sample CP-3, a parallel-laminated swale drape. (A) shows sample CP-3 in outcrop, extracted from the base of a swale drape. (B) shows the sample in thin section, the white arrow pointing to a relatively coarser silt lamination. The brownish matrix above the sequestration is a bed of diatomite containing finer silt. Note the relatively pure diatomite that occurs just under the silt sequestration at the white arrow, marking the cap of a previous deposit. (C) shows smaller, sucessive couplets at the laminae scale. (D) is a magnification of (C), showing the grading among the silt component of the couplets. Note that the coarse silt sequestration is diatom-poor, fining upward into intercalated silt-diatomite. The coarse lamina represents the tail of a migrating silt ripple, while the intercalation above represents the migration paths of successive diatomaceous floccule ripples with fine silt inclusion.

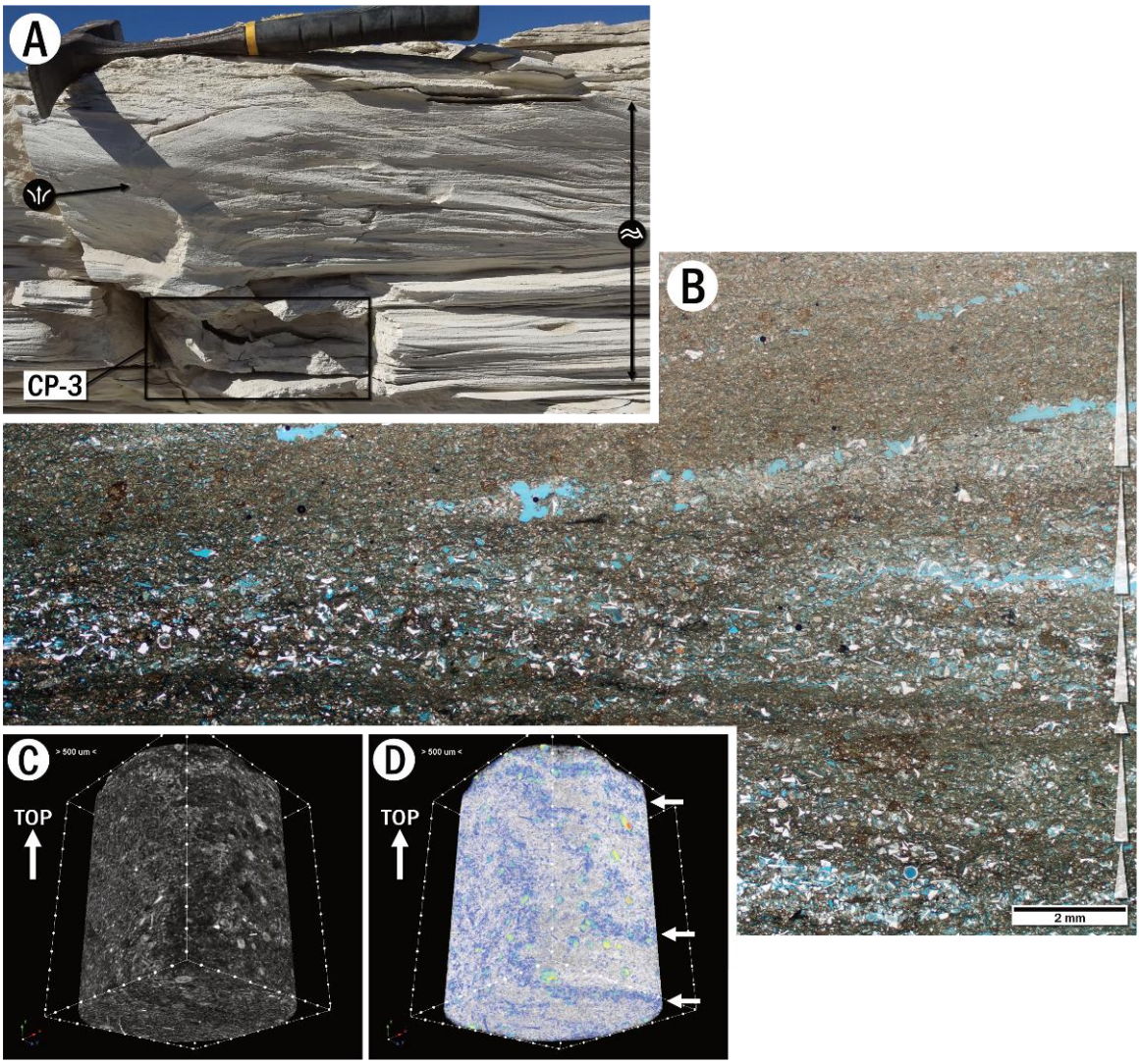

Figure 11. Overview of sample CP-4 in outcrop (A), showing syndepositional soft-sediment deformation in hummocky-swaley cross-laminated diatomite. (B) shows a less-deformed interval in thin section. Lamina show a couplet architecture where coarser ash fines upward into finer silt-diatomite. Note gentle pinching-out toward the left. Eccentric pores are an artifact of thin section preparation where larger silt grains have been plucked during processing. A micro-CT surface model of deformed couplets can be seen in (C) looking up from below. In (D), the diatomaceous component has been thresholded and rendered white while silt sequestrations (arrows) have been 'heat-mapped' for size. Larger sequestrations appear as more red, smaller as bluer. This illustrates that primary depositional and tractional textures can survive deformation. Scan taken at 5 µm resolution. Diatom grey value thresholded from 35-90. Silt and denser minerals highlighted from 90-255. Silt sequestrations color-coded for size over trabecular thickness.

Location 3: Cerro Mamá y la Hija: Interlaminated Stacked Channel Complex

At Cerro Mamá y la Hija, a stacked channel complex cutting into an apparently muddy lithology was observed, its infill composed of interlaminated diatomite-siltstone. Laminae were texturally revealed to be non-discrete, with several showing the same couplet to triplet architecture observed elsewhere in the Pisco but in a siltier lithology. Within channel (Figure 12A), lamina geometry varies from base to top, starting as largely continuous and planar, proceeding upward to become wavier and more discontinuous (Figure 12B). The very top of the uppermost channel appeared churned by bioturbation with several burrows extending further into the channel below the churned contact. Above, the complex is apparently truncated by a coarser lithology.

Texturally, laminae mainly exhibit couplet to triplet architecture, containing a normally graded silt component composed of quartz, feldspars, and ash that is reverse graded to capped with diatomite. In thin section, lamina geometry appears as variable as in outcrop, showing convolute to continuous to gently pinching out structure (Figure 12C). An exceptionally graded interval is illustrated in Figure 12D, a triplet composed of a relatively coarse, basal siltstone fining upward into a mix of siltstone-diatomite and capped with pure diatomite. Consequentially, pore size is reverse graded within couplet and triplet laminae (Figure 12F).

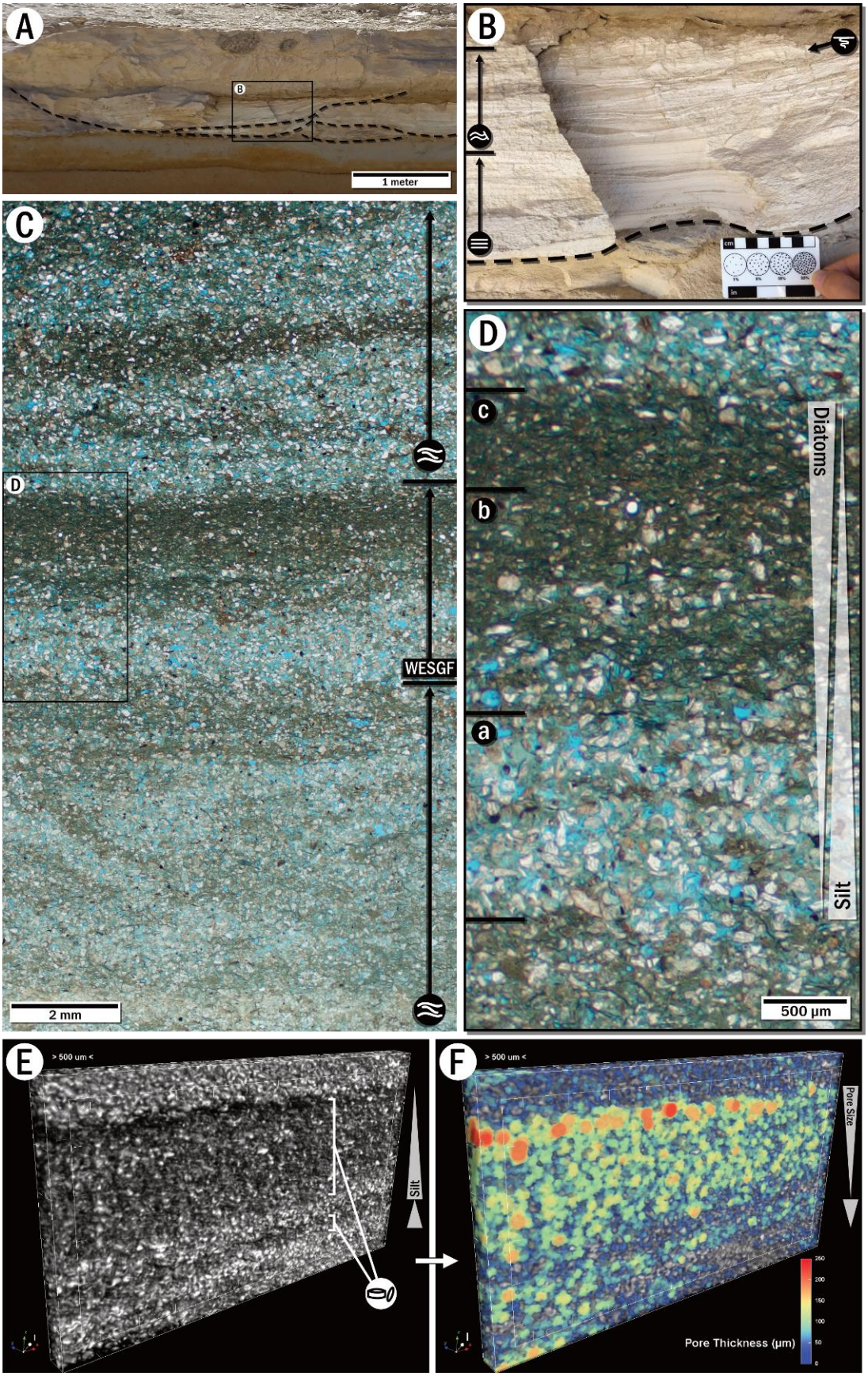
A
B
1 meter
B
C
D
WESGF
2 mm
D
c
b
a
Diatoms
Silt
500 µm
E
> 500 um <
Silt
F
> 500 um <
Pore Size
Pore Thickness (µm)

Figure 12. Overview of an interlaminated channel complex at Cerro Mamá y la Hija. (A) shows the complex in outcrop with channel bases outlined by the dashed lines. (B) shows channel in-fill, consisting of alternating laminae of diatomite-siltstone, later revealed to be graded micro-couplets. In outcrop, it also grades upward from more planar laminated at channel base to hummocky-like as in-fill proceeded. The top is mildly bioturbated. In thin section (C), couplets can be seen conforming to a variety of fabrics including convolute (lower half of image), low-angle hummocky (top of image, note gentle pinching-out). Graded triplets can also be seen, their architecture characteristic of wave enhanced sediment gravity flows (WESGF). In (D), one WESGF is magnified, its graded triple composed of a basal siltstone 'a', grading upward into a mix of diatoms and silt 'b', and capped with relatively pure diatomite 'c'. WESGF's are a product of sediment entertainment by storm waves to produce a higher-density fluid that moves downslope (Lazar et al. 2015). The micro-couplets seen here are interpreted as the product of the tandem migration of silty and diatomaceous floccule ripples, or as previous WESGFs scoured down to couplets instead of triplets by successive flows. (E) shows a maximum intensity projection of a micro-CT model to isolate the higher-density, silt component of a lower couplet and overlying triplet, further illustrating grading. In (F), pore size has been 'heat-mapped' to the model, showing a reverse grading in pore size that is greatest within the diatomaceous caps of couplets and triplets alike. Scan taken at 5 μm resolution. Rock isolated by a contrast enhancement filter and automatic Otsu thresholding. Pore size calculated via trabecular separation calculation.

Interpretations

Location 1: Cerro Hueco la Zorra: Cross Laminated Diatomite

Five, approximately 1 mm thick laminae are captured in Figure 6A, three showing downlapping micro-foresets and two showing wavy, non-parallel and discontinuous internal micro-laminae. The laminae containing downlapping micro-foresets are interpreted as current ripples migrating across the field of view, presumably driven under unidirectional flow (Schieber and Southard, 2009; Schieber and Yawar, 2009; Yawar and Schieber, 2017). Figure 6B magnifies a set of climbing ripples showing internal sorting by way of graded micro-couplets where relatively coarser silt fines upward into finer silt and a condensed cap of diatoms that are mostly centrics. Graded micro-couplets were observed in many other samples from several locations across the Pisco formation. These mostly occur as laminae or lenses (Figures 10, 11, 6), but here, couplets appear to downlap along with ripple accretion. Figure 6C shows perhaps the most distinct set of micro-foresets present in a wedge that appears to follow scoured and truncated laminae deposited over wavy lamina.

The wavy, non-parallel laminae of Figure 6 prove more difficult to interpret due to their discontinuity. These could represent current-ripple migration transverse to the field of view (Lazar, 2015, pp. 24-25), and thus could be interpreted as low-angle, trough cross-stratification. If true, it would mean that the unidirectional current which deposited the sample shows considerable variance in its flow direction over very short spans of deposition. This interpretation is perhaps supported by the downlapping forests seen at apex of Figure 6A, D, downlapping left in opposition to the rest of the fabric, which tends to downlap to the right.

Alternatively, some micro-laminae of the wavy intervals show plausible onlap, and if accurate, suggest the possibility that oscillatory flow may have played a part in their deposition (Lazar 2015, pp. 26-27). If true, this interpretation suggests a predominantly unidirectional flow intermittently interrupted by passing waves, and therefore, possibly represents deposition from combined flow. This interpretation is seemingly supported by the occurrence of hummocky-swaley cross-stratification in the diatomaceous siltstone and diatomite outcrops of the Pisco (Figures 4B; 7; 9; 10; 11). These structures are associated with combined-flow and waning storm conditions (Dott and Bourgeois, 1982; Dumas, 2006, Myrow et al., 2002), conditions which were apparently frequent over the Formation's deposition. Thus, this micro cross-laminated fabric may represent the exceptional preservation of a combined-flow fabric at the sub-lamina scale.

An alternative interpretation of these textures involves bioturbation. Burrowed mudstones have also been reported to exhibit micro-cross-laminated fabrics. Lazar (2015, pp. 60-62) presents an example of a coarse mudstone microfacies from the Eastern Triangle Formation (Upper Devonian Sonyea Group of New York) whose laminae are interpreted as a product of bioturbation by *Zoophycos*. Bioturbation resulted in clay-lined and silt back-filled burrows whose migration across successive horizons has created a cross-laminated fabric. However, this upper Devonian example does not occur in diatomaceous lithologies which are typically highly porous, fluidized, and inhospitable to bioturbators on account of both diatom frustule porosity and rigidity (Kemp, 1993). Likewise, evidence of clay- to diatom-lined burrows with silty back-fill were not observed in sample CHZ-1, whereas signs of tractional sorting (Figure 6B) and locally

uniform foreset migration (Figure 6C) remain compelling indicators of a tractional genesis.

Location 2: Cerro Pileta: Storm-Dominated Diatomite

The identification of these features as swales and hummocks is certainly surprising given their lithologic association, yet in outcrop, these structures appear well-distributed, frequently truncating one another, and appear largely isometric in form. Thus, this and other studies (Flemming, 2014) have chosen to describe the diatomite and diatomaceous siltstone of Cerro Pileta as bearing hummocky-swaley cross-stratification, a product of sedimentation during waning storm conditions under a combined-flow (Dumas, 2006). By inspection, convex-up, swaley features tend to predominate over hummocky, mirroring bedforms and sequences observed by Myrow et al. (2002) which were interpreted as the product of current-dominated combined flows, or rather, wave-modified turbidity currents. While more planar laminated and hummocky-swaley intervals do occur in outcrop in some places, the homogenous lithology of Cerro Pileta makes obvious signs of grading or Bouma-like sequences ambiguous, and thus, the exact intersection of density-induced flow, wave oscillation, and geostrophic current derived from outcrop observations remains difficult to say with certainty (Dumas, 2006; Myrow, 2002).

With regards to micro-texture, this study attributes the high-degree of fragmented diatom frustules within the micro-matrix across samples as a product of successive exhumation and reworking, possibly over several storm cycles. Those diatoms which do occur articulated and well-preserved are more likely to have undergone primary

deposition or fewer cycles of reworking. Such whole individuals may have met a similar fate to Cerro Pileta's fossil whales, buried and preserved (though well-compacted) in a fabric composed of their less fortunate compatriots.

Likewise, the pennate diatom mats seen in Figures 8 and 9 are interpreted to reflect varying states of mat break-up from larger fragments down to the discrete 'bundles' which compose the mat's fabric. Similar mat fragments composed of entire frustules, pieces of frustules, and filaments were observed by Esperante (2002), postulated (though not asserted) to be fragments of larger mats that may have once covered meters to perhaps tens of meters across the sea bottom that were broken up and associated with scour-and-fill structures in his study (pp.139-140). However, it remains entirely possible that the variation in scale between the mat and individual bundles may simply reflect variance in natural diatom proliferation. Kemp and Baldauf (1993) observed laminated oozes of Neogene pennate diatoms of the equatorial Pacific as individuals, colonial bundles, and more cohesive mats alike, almost assuredly deposited as a product of hemipelagic sedimentation over the deep ocean. Yet, at Cerro Pileta, given the ubiquitous, storm-derived fabrics observed in outcrop, the mat fragments' suspension within a highly fragmented micro-matrix, and presence of traction-derived, graded silt sequestrations, it remains possible that mat break-up was, at least to some degree, enhanced by storm action.

The diatomite of Cerro Pileta is observed as a composite of micro-couplets showing internal grading by way of a basal sequestration of relatively coarser silt fining upward into an intercalated matrix of diatoms containing finer silt inclusions (Figures 10, 11). This remains the most apparent evidence for tractional deposition of Cerro Pileta's

diatomite, mirroring textures derived from flume experiments by Yawar and Schieber (2017). In those experiments, clay-silt mixtures were used to accrete interlaminated, muddy beds where relatively coarser silt was shown to sequester as laminae and lenses, suspended in an intercalated matrix of finer silt and flocculated clay. Silt sequestration was interpreted as a product of sorting, while interlamination was the result of the tandem and random migration of silt-rich and clay-floccule ripples containing fine-silt inclusions. As clay-floccule ripples migrate overtop the tails of coarser silt ripples, a fining upward profile is formed composed of a silt-clay couplet.

Due to its similarity in texture and fabric, the diatomite of Cerro Pileta may have undergone a similar mode of deposition, albeit due to the tandem migration of silt-rich and diatomaceous floccule ripples, where pulses of diatoms and silt, entrained by storm waves, were delivered toward the offshore by bedload transport and ripple migration. The mechanism of flocculation would differ in a diatomaceous substrate over the dominantly electrostatic interactions defining clay particle flocculation. Presumably, an interlocking of spines, pores, and processes alongside mutual mucilage adhesion would allow for diatom aggregation, flocculation, and entrainment during bedload transport. The pennate aggregates and bundles seen in Figures 8, 9, interpreted as mat fragments, remain the most obvious remnants of flocculated diatoms. If mats were living at the time of storm onset and break-up, their fragments could have acted as floccule nucleation sites. However, apart from the monospecific, pennate aggregates, mixed diatom aggregates remain either obscure, unapparent, or absent in the diatomaceous matrix of Cerro Pileta. Both diatoms and clays can be highly fluidized upon deposition, and as seen in clays,

signs of flocculation can be overwritten by compaction (Lazar, 2015; Yawar and Schieber, 2017).

Note that the experiments of Yawar and Schieber (2017) involve only unidirectional currents, only one component of the apparent combined-flow fabrics witnessed in outcrop. In the case of our swale draping (Figure 10), it is interpreted that silt and diatomaceous floccule ripples were left largely protected and uninterrupted by oscillatory currents in their accretion, producing a mostly uniform, planar laminated fabric. However, the bulk of laminae observed at Cerro Pileta are wavy and moderately continuous to discontinuous, resembling combined-flow fabrics (Figures 7, 9, 11). This is interpreted as the product of floccule ripple migration driven mainly by the unidirectional component of combined-flow where ripple migration is interrupted by the oscillatory component of flow, causing ripples to truncate one another and form combined-flow lamination. Therefore, it may be that the unidirectional component of combined flow is what largely defines micro-texture while varying inclusion of the oscillatory component works to define overall bed to lamina-set structure.

Overall, storm-dominated depositional conditions for this diatomite are both implied by micro-texture and the presence of interpretable tempestite sequences (based on Dott and Bourgeois, 1982) defined by extensive basal scour and accompanying lags (note Figure 7C, the fossil whale interpreted as a basal lag) and overlain by hummocky-swaley cross-stratified deposits. Progressively, these mark storm onset and scour followed by waning sedimentation, the swales across the scoured seafloor being some of the first structures to be draped by bedload-entrained sediments and diatoms as they migrate towards the offshore. The combined-flow regime works to produce large

successions of hummocky-swaley cross-stratification, possibly amalgamated due to varying storm conditions or successive storm events (Dott and Bourgeois, 1982), with a dominance of swaley cross-stratification either due to a prominence of scour over deposition (Dumas, 2006) or current-dominant combined-flow (Myrow, 2002). At the level of micro-texture, individual laminae are deposited as graded micro-couplets across structures reflecting, at the very least, the unidirectional component of combined flow. Silt and diatoms were deposited largely unconsolidated, with soft-sediment deformation possibly resulting from gravity-driven instability of water-saturated sediments (Myrow, 2002), particularly acute due to the high porosity of diatom frustules (Kemp, 1993). Forced by overburden, fluid escape, lamina deformation and compaction follow (Shanmugam, 2017), though original lamina texture may be preserved.

Location 3: Cerro Mamá y la Hija: Interlaminated Stacked Channel Complex

This study proposes two explanations for the style of stratification seen at the outcrop scale of channel infill. The first explanation is inferred from the frequent occurrence of storm stratification within the Pisco. It interprets the wavy, non-parallel lamination seen at the top of the channel as hummocky-swaley cross-stratification. During a storm, the channel may be eroded by the unidirectional component of combined flow. This current simultaneously carries density-laden pulses of silt and diatoms, entrained by storm waves, down the channel and away from shore. These hyperpycnal-like flows may also work to carve the channels themselves (Mulder er al., 2003). These pulses are deposited largely as couplets but also as triplets where sediment entrainment is exceptional enough to produce a wave-enhanced sediment gravity flow (Lazar, 2015, pp. 30-31; Macquaker et al., 2010). Infill remains largely planar at the base, affected solely

by the unidirectional component of flow, but becomes more hummocky-swaley as the channel is filled, its sediment exposed to the overriding, oscillatory component of combined flow (Dumas, 2006). The bioturbated top completes the tempestite sequence as post-storm infaunae recolonize the seafloor (Dott and Bourgeois, 1982). Rapid channel infill has apparently protected the majority of its sediment from overprint.

Alternatively, the channel complex could be placed at a location more distal from shore, possibly below storm-wave-base. This inference is supported by the apparently massive and muddy lithology into which the channel complex is cut. Storm wave sediment entrainment is still proposed as the mechanism by which sediments are delivered offshore. However, only the bottom-hugging unidirectional component of flow (Dumas 2006) is invoked in couplet and triplet deposition. At the initial stages of sedimentation, sediment supply is high, resulting in transverse ripple migration down channel and the deposition of planar lamination at its base. As sediment supply decreases, transverse ripples progressively change into a barchanoid style of ripple (see Yawar and Schieber 2017, their Figure 23). Thus, the wavy, non-parallel laminae at the top of the channel are interpreted here as barchanoid ripples in transverse view. Intermittently, a wave enhanced sediment gravity flow may interrupt ripple deposition, but ripple migration continues in its wake. Infaunal colonization occurs once quieter conditions resume.

Deep-Sea Diatomite: A Brief Comparison

A few diagnostic differences are expected between shallow shelf and deep-sea diatomite. A literature review by Wiemer et al. (2017) revealed a near systematic over-consolidation of shallow shelf diatomaceous sediments, whereas deeper sequences remained largely normally to under-consolidated. Fabric analysis of laminated diatom ooze was conducted by Grigorov et al. (2002) on samples collected in the Southern Ocean between Africa and Antarctica during ODP Leg 177. Their analysis revealed a couplet-triplet architecture among laminae; however, these were interpreted as possibly reflecting annual cyclicity as couplets were composed of pure mats of the pennate diatom *Thalassiothrix antarctica*, followed by a mixed centric/fragmented pennate lamina. Furthermore, they conclude, "Compared to laminated sediments from marginal marine basins, the examined intervals lack significant terrigenous input and are entirely biogenic in origin. Variations in diatom species and the degree of fragmentation seem to be the main causes of persistent submillimetre laminations." Mat-dominated laminae are apparently the best preserved, though partially fragmented, etched, and pitted diatoms of all types were observed throughout the sediment, interpreted as possibly reflecting differential dissolution during settling or subsequent bioturbation and disturbance. However, from inspection of published SEM images (Grigorov, 2002, their Figure 4), both frustules and frustule fragments appear markedly more complete than the highly abraded, micro-matrix of diatom hash found in the Pisco diatomite by this study (Figures 8C, D) and others (Stanton, 2014).

Conclusions

Within the Pisco formation and the three locations visited, laterally transported and reworked diatomite to diatomaceous siltstone is present. At Cerro Hueco la Zorra, cross-laminated diatomite containing both climbing ripples and migrating foresets were found preserved, some of which were internally graded as a set of downlapping micro-couplets. At Cerro Pileta, extensive deposits of longitudinally bedded hummocky-swaley cross-stratified diatomite intermixed with ash were found to contain silt sequestrations as lamina and lenses overlain by a diatomite. These were also interpreted as graded couplets and the product of tractional sediment transport under combined-flow generated by storm conditions. Lastly, at Cerro Mamá y la Hija, the interlaminated infill of diatomite-siltstone within a stacked channel complex was found to be a composite of graded couplets to triplets as well, attributed to cyclical pulses of sediment entrained by storm waves to form a higher density fluid before being driven offshore and down channel. The application of micro-CT analysis proved instrumental in the volumetric identification of micro-couplets and triplets, namely by way of pore size mapping and color-coding, which clearly revealed a consistent, internal grading that was initially obscured in thin section and SEM imaging.

Based on these findings, it is urged that future studies take caution in assigning a low-energy depositional environment to diatomite based on lithology alone. The depositional parameters associated with mudstones have been largely overturned in recent decades, leading to an understanding that deposition can occur under higher-energy conditions than previously assumed (Bohacs, 2014; Lazar, 2015; Schieber, 2007; Schieber and Southard, 2009; Schieber and Yawar, 2009; Yawar and Schieber, 2017), and it would appear that diatomite may accumulate under similar regimes, and in

exceptional cases, may do so in significant successions. The findings of this study may be most applicable to the diatomaceous Miocene analogs of the Pisco formation occurring around the Pacific margin.

Future researchers in the Pisco and beyond may wish to include textural observations in conjunction with diatom biostratigraphy in order to assure those stratigraphic horizons are not reworked and reflect discrete, non-mixed assemblages. Likewise, future studies should taxonomically evaluate reworked horizons of diatomite to ensure that their diatom content reflects a mixed assemblage, the samples and locations detailed in this study included. Since events of reworking are potentially punctuated, such work would help establish a proper resolution with which to apply diatom biostratigraphy, though that would have to be coupled with sedimentology and recognition of, in the case of the Pisco, tempestite boundaries. Degrees of reworking may also affect source or reservoir quality, and if correlated, may prove a predictive variable in assessing a formation's economic potential. Thus, more accurately assessing diatomite's texture, taxonomic composition, and sedimentological superposition may prove as instrumental, and possibly predictive, in refining observations, constraints, and processes in broader diatomaceous sequences and formations as well as the conditions defining their entrainment and deposition.

References

Brand, L. R., Esperante, R., Chadwick, A. V., Porras, O. P., & Alomía, M. (2004). Fossil whale preservation implies high diatom accumulation rate in the Miocene–Pliocene Pisco Formation of Peru. Geology, 32(2), 165-168.

Bohacs, K. M., Lazar, O. R., & Demko, T. M. (2014). Parasequence types in shelfal mudstone strata—Quantitative observations of lithofacies and stacking patterns, and conceptual link to modern depositional regimes. Geology, 42(2), 131-134.

Cobbing, E. J. (1999). The Coastal Batholith and other aspects of Andean magmatism in Peru. *Geological Society, London, Special Publications*, *168*(1), 111-122.

de Muizon, C., & Devries, T. J. (1985). Geology and paleontology of late Cenozoic marine deposits in the Sacaco area (Peru). *Geologische Rundschau*, *74*(3), 547-563.

Di Celma, C., Malinverno, E., Bosio, G., Collareta, A., Gariboldi, K., Gioncada, A., ... & Pierantoni, P. P. (2017). Sequence stratigraphy and paleontology of the Upper Miocene Pisco Formation along the western side of the lower Ica Valley (Ica Desert, Peru).

Dott Jr, R. H., & Bourgeois, J. (1982). Hummocky stratification: significance of its variable bedding sequences. Geological Society of America Bulletin, 93(8), 663-680.

Dumas, S., & Arnott, R. W. C. (2006). Origin of hummocky and swaley cross-stratification—The controlling influence of unidirectional current strength and aggradation rate. *Geology*, *34*(12), 1073-1076.

Dunbar, R. B., Marty, R. C., & Baker, P. A. (1990). Cenozoic marine sedimentation in the Sechura and Pisco basins, Peru. *Palaeogeography, Palaeoclimatology, Palaeoecology*, *77*(3-4), 235-261.

Esperante, R. (2002). Taphonomy of Fossil Whales in Diatomaceous Sediments of the Neogene Pisco Formation, Peru (Doctoral dissertation). Loma Linda University, Loma Linda, CA.

Esperante, R., Brand, L. R., Chadwick, A. V., & Poma, O. (2015). Taphonomy and paleoenvironmental conditions of deposition of fossil whales in the diatomaceous sediments of the Miocene/Pliocene Pisco Formation, southern Peru—A new fossil-lagerstätte. Palaeogeography, Palaeoclimatology, Palaeoecology, 417, 337-370.

Fleming, M. A. (2014). Sedimentology of Marine Vertebrate Burial in the Miocene Pisco Fm., Peru (Master's thesis). Loma Linda University, Loma Linda, CA.

Gariboldi, K., et al. (2017). Biostratigraphy, geochronology and sedimentation rates of the upper Miocene Pisco Formation at two important marine vertebrate fossil-bearing sites of southern Peru. Newsletters on Stratigraphy 50(4): 417-444.

Grigorov, I., Pearce, R. B., & Kemp, A. E. (2002). Southern Ocean laminated diatom ooze: mat deposits and potential for palaeo-flux studies, ODP leg 177, Site 1093. Deep Sea Research Part II: Topical Studies in Oceanography, 49(16), 3391-3407.

Ingle Jr, J. C. (1981). Origin, Depositional History, and Correlation of Miocene Diatomites Around North Pacific Margin. AAPG Bulletin, 65(5), 940-940.

Kemp, A. E., & Baldauf, J. G. (1993). Vast Neogene laminated diatom mat deposits from the eastern equatorial Pacific Ocean. Nature, 362(6416), 141-144.

Lazar, O. R., Bohacs, K. M., Schieber, J., Macquaker, J. H., & Demko, T. M. (2015). Mudstone Primer: Lithofacies variations, diagnostic criteria, and sedimentologic-stratigraphic implications at lamina to bedset scales. SEPM (Society for Sedimentary Geology).

Macquaker, J. H., Bentley, S. J., & Bohacs, K. M. (2010). Wave-enhanced sediment-gravity flows and mud dispersal across continental shelves: Reappraising sediment transport processes operating in ancient mudstone successions. Geology, 38(10), 947-950.

Mulder, T., Syvitski, J. P., Migeon, S., Faugeres, J. C., & Savoye, B. (2003). Marine hyperpycnal flows: initiation, behavior and related deposits. A review. Marine and Petroleum Geology, 20(6-8), 861-882.

Myrow, P. M., Fischer, W., & Goodge, J. W. (2002). Wave-modified turbidites: combined-flow shoreline and shelf deposits, Cambrian, Antarctica. Journal of Sedimentary research, 72(5), 641-656.

O'Brien, N. R., & Slatt, R. M. (1990). *Argillaceous rock atlas*. Springer Science & Business Media.

Pilger JR, R. H. (1981). Plate reconstructions, aseismic ridges, and low-angle subduction beneath the Andes. *Geological Society of America Bulletin*, *92*(7), 448-456.

Püspöki, Z., Storath, M., Sage, D., & Unser, M. (2016). Transforms and operators for directional bioimage analysis: a survey. In Focus on Bio-Image Informatics (pp. 69-93). Springer, Cham.

Schieber, J., Southard, J., & Thaisen, K. (2007). Accretion of mudstone beds from migrating floccule ripples. Science, 318(5857), 1760-1763.

Schieber, J., & Southard, J. B. (2009). Bedload transport of mud by floccule ripples—Direct observation of ripple migration processes and their implications. Geology, 37(6), 483-486.

Schieber, J., & Yawar, Z. (2009). A new twist on mud deposition: mud ripples in experiment and rock record. The sedimentary record, 7(2), 4-8.

Shanmugam, G. (2017). Global case studies of soft-sediment deformation structures (SSDS): Definitions, classifications, advances, origins, and problems. Journal of Palaeogeography, 6(4), 251-320.

Stanton, C. (2014). Correlation and Paleoenvironments above West T9. 3 Tuff, Pisco Formation, Peru (Master's thesis). Loma Linda University, Loma Linda, CA.

Thornburg, T. M., & Kulm, L. D. (1981). Sedimentary basins of the Peru continental margin: Structure, stratigraphy, and Cenozoic tectonics from 6 S to 16 S latitude. *Geological Society of America Memoir*, *154*, 393-422.

Thornton, D. C. (2002). Diatom aggregation in the sea: mechanisms and ecological implications. European Journal of Phycology, 37(2), 149-161.

Wiemer, G., & Kopf, A. (2017). Influence of diatom microfossils on sediment shear strength and slope stability. Geochemistry, Geophysics, Geosystems, 18(1), 333-345.

Yawar, Z., & Schieber, J. (2017). On the origin of silt laminae in laminated shales. Sedimentary Geology, 360, 22-34.

CHAPTER THREE

CLOSING REMARKS AND FUTURE RESEARCH

Concerning the research inscribed in this document as a whole, several congruent paths for future research are apparent. The first of which concerns the particulars of diatom flocculation during transport (or more generally aggregation, presuming diatoms do aggregate during transport at all). Most studies up until this point seem more concerned with diatom flocculation and sinking rates within a passive setting. While many diatomite textures observed here mirror those observed and experimentally derived in flume experiments of migrating floccule ripples, it needs to be affirmed that diatoms can flocculate and deposit in a manner effectively similar to clays, therefore producing similar depositional textures. Diatomaceous flume experiments should be conducted to examine this.

Diatomaceous, Miocene analogs to the Pisco Formation should also be reevaluated for signs traction-derived textures and other signs of reworking. If reworked textures are present, the application of high-resolution diatom biostratigraphy is cautioned though that will largely depend on the severity of reworking. Conceptually, reworking should tend to drive down diatomite's porosity and permeability due to diatom fragmentation, while also liberating any previous sequestered organic matter as well. Therefore, it may be useful to establish an index of reworking or degrees of reworking to describe diatomaceous sediments as this may relate to their potential to become either a reservoir, seal, or source rock.

APPENDIX

TEXTURAL ATLAS FOR THE PISCO DIATOMITE

Concerning the Appendix: Textural Atlas for the Pisco Diatomite

The intent of this appendix is to provide a textural atlas for all the samples of the Pisco diatomite not included in Chapter Two of this document. The same three locations are used as subdivisions with one additional location added: Cerro Ballena. Consequentally, Cerro Ballena diatomite was also found to contain depositional textures that could be interpreted as reflecting a tractional genesis despite most outcrops appearing massive to faintly laminated. An appended aerial image of East Pisco Basin is provided on the following page, followed by a generalized template for the atlas roughly based on "Templates for Capturing Key Attributes of Mudstones in Thin Sections" found in Lazar et al. (2015, pp. 177-181). Each page describes one sample in detail, including the outcrop it is from and its depositional texture in thin section. Some samples also include SEM images and micro-CT models. Depositional processes per sample are briefly considered.

Oblique Aerial of East Pisco Basin

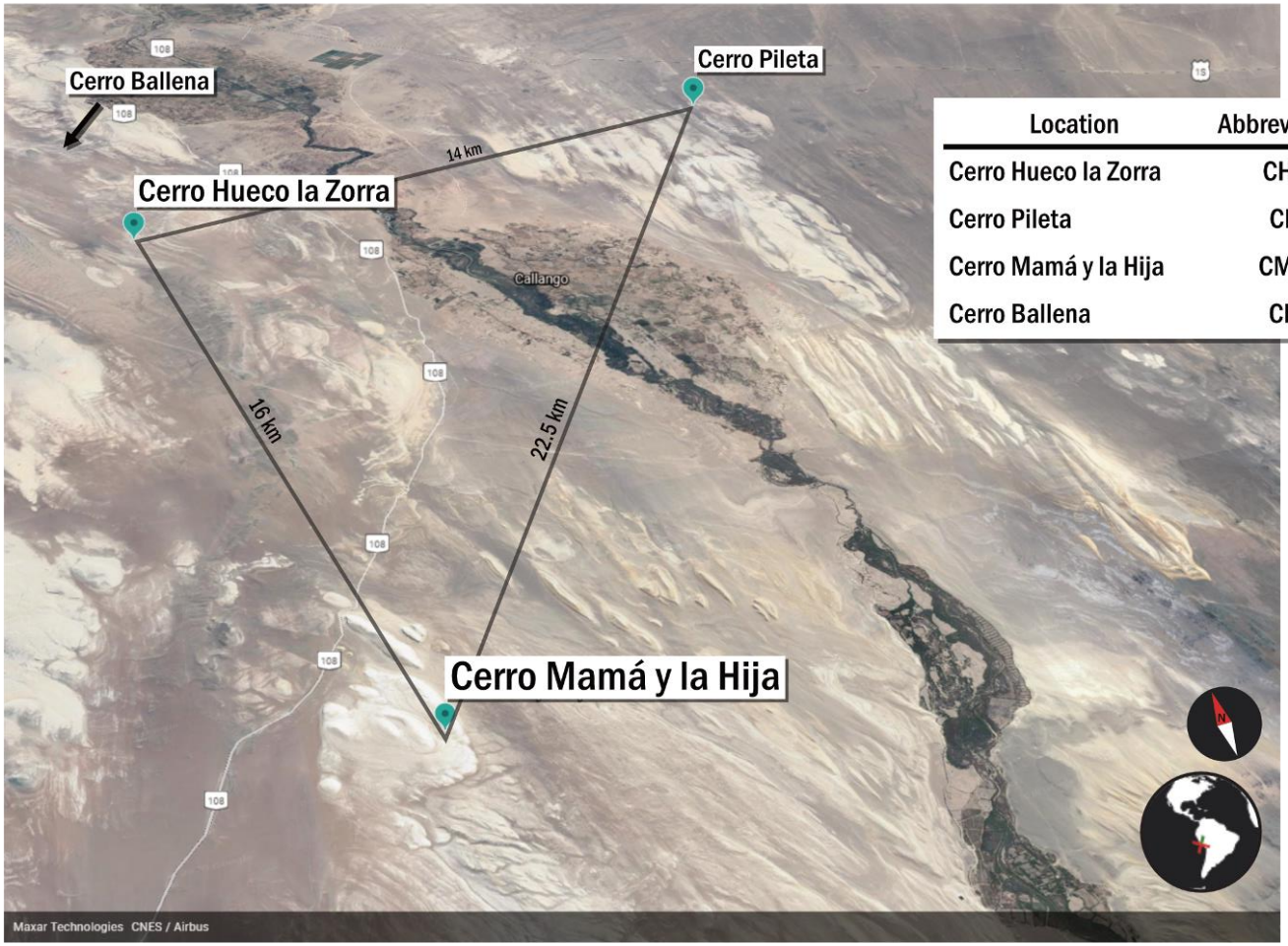

Location	Abbreviation	GPS
Cerro Hueco la Zorra	CHZ	-14.46426° -75.70051°
Cerro Pileta	CP	-14.43179° -75.57683°
Cerro Mamá y la Hija	CMH	-14.61005° -75.67668°
Cerro Ballena	CB	-14.35522°,-75.71764°

Location / Sample ID / GPS

(General template)

Outcrop photo

SEM image

Outcrop description:

Texture:

Lamina geometry:

Physical sedimentary structures:

Other:

Interpretation:

Thin section image

Cerro Ballena / CB-1 / -14.35529,-75.71765

Outcrop description: Off-white to tanish-pink in color, massive to faintly laminated

Texture: Silty diatomite

Lamina geometry: Mostly continuous and parallel; some discontinuous and curved

Physical sedimentary structures: Silt laminae, lenses (white arrows); normally graded lamina

Other: Large centrics compacted with the horizontal, some show possible imbrication (note bottom of SEM)

Interpretation: Presence of normally graded silt laminae and lenses suggest a possible genesis via floccule ripple migration. Dominance of lenses suggests low sediment supply and rates, producing a barchanoid style of ripple (Yawar and Schieber, 2017). Gently dipping silt lenses may conform to crests of underlying ripples.

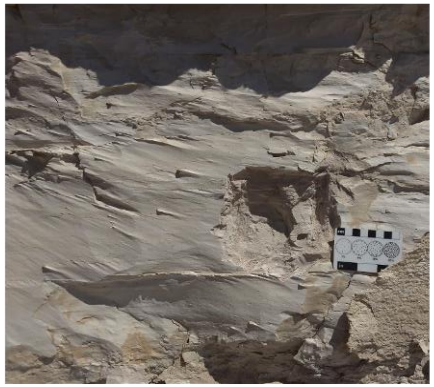

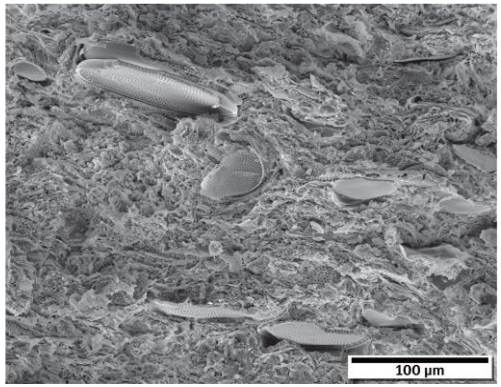

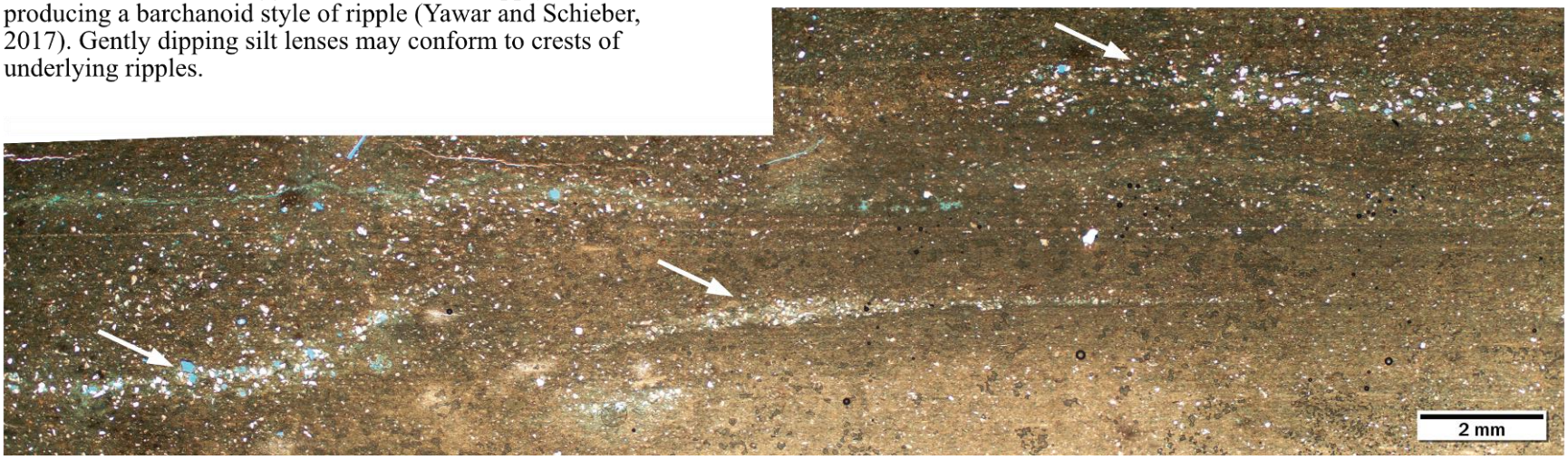

Cerro Ballena / CB-2 / -14.35524,-75.71764

Outcrop description: Bright white with some orange staining, massive to planar laminated (sample taken near yellow arrow)

Texture: Silty diatomite

Lamina geometry: Continuous, parallel, but mostly massive as a result of high diatom content and lack of coarser silt

Physical sedimentary structures: Silt laminae (black arrows)

Other: Appears centric-dominated, few radiolarians present

Interpretation: Presence of silt lamina suggests possible genesis via floccule ripple migration (Yawar et al., 2017).

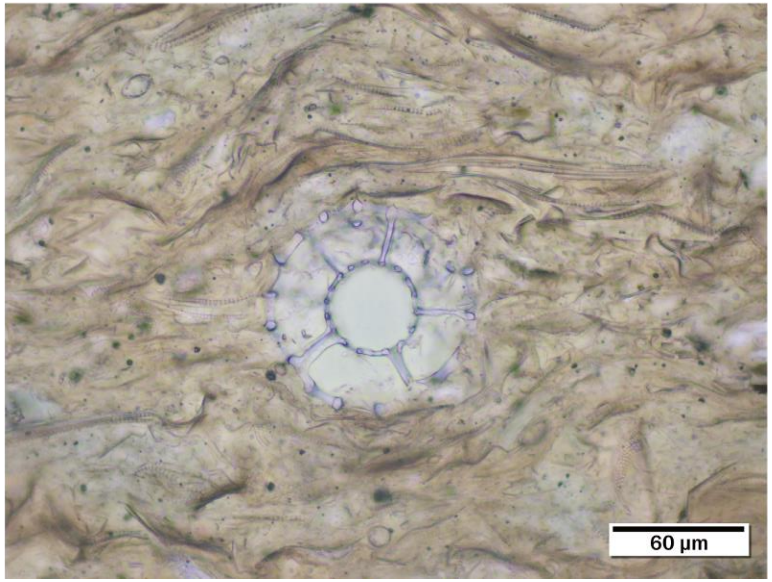

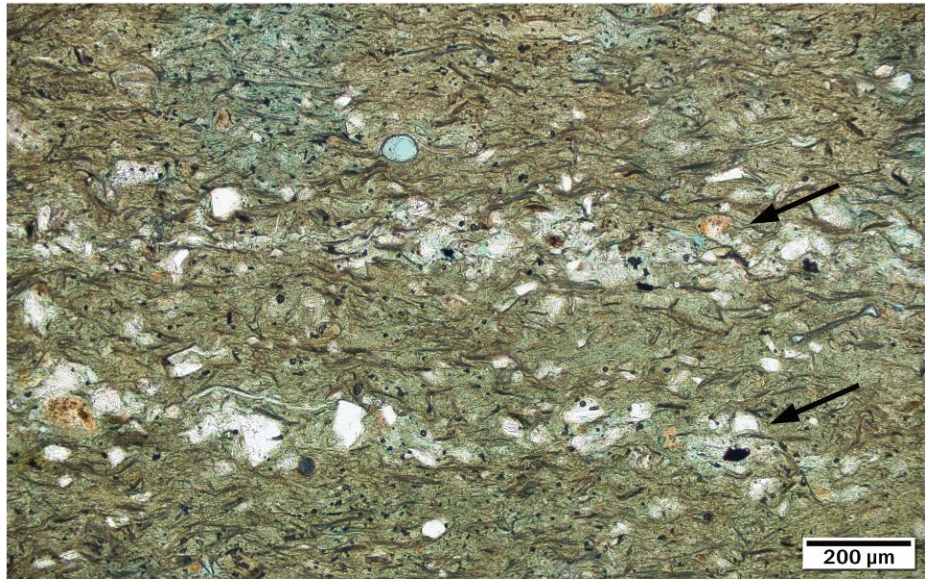

Cerro Ballena / CB-3 / -14.35522,-75.71764

Outcrop description: Off-white with some bright white laminae and specks (possibly diatom mats?)

Texture: Silty diatomite interlaminated with pure diatomite

Lamina geometry: Planar, parallel, mostly continuous with faint signs of truncation in outcrop (note yellow arrow)

Physical sedimentary structures: Silt lens (white arrow), possible grading, condensed laminae rich in centric diatoms (between black arrows)

Other: Appears centric-dominated, frustules deform about silt grains more distinctly than in other samples (note similarity to dropstones)

Interpretation: Two interpretations are posited for this sample. A tractional genesis can be infered from the silt lense, possibly grading upward and capped in a condensed laminae of centric diatoms. Thus, these would be considered something approaching sediment gravity flow deposits. However, the dropstone-like appearance of silt within the sample more acute than in others and seems to suggest silt settling out alongside the diatom content. If this truly represents suspension settled diatomite, then the condensed centric laminae alternating with more silt-rich laminae may represent something approaching varves with increased silt input from rivers during wet months and capped with pure diatoms during dry months.

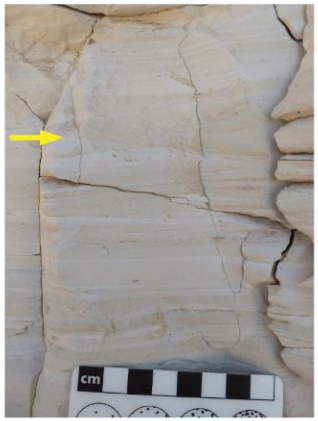

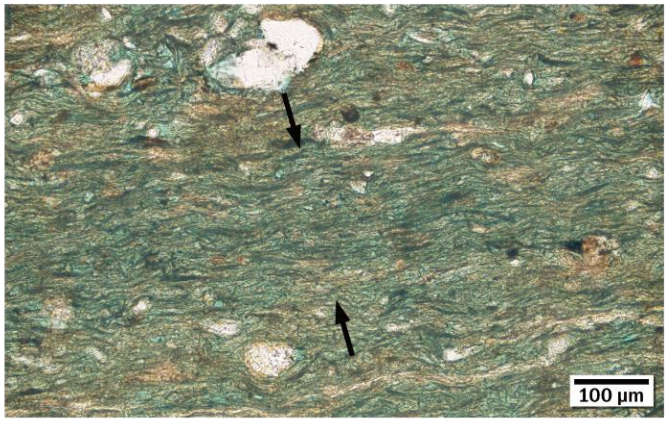

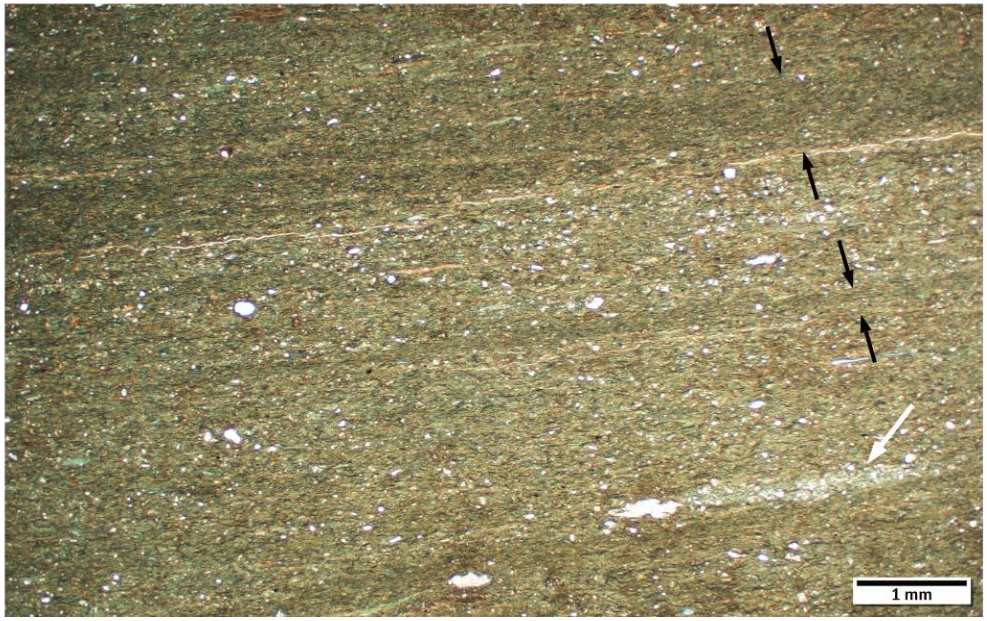

Cerro Hueco la Zorra

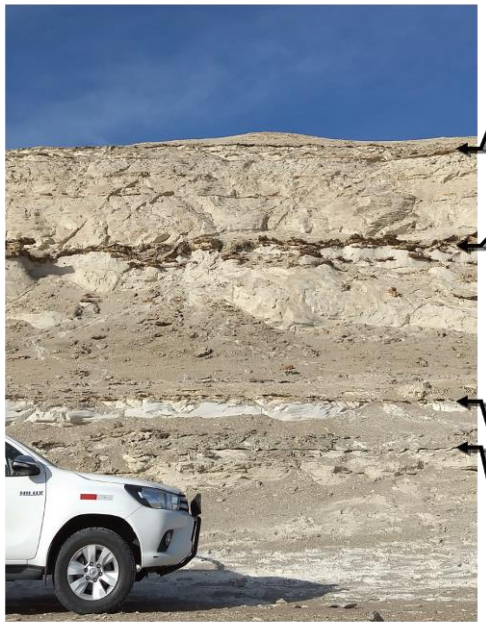

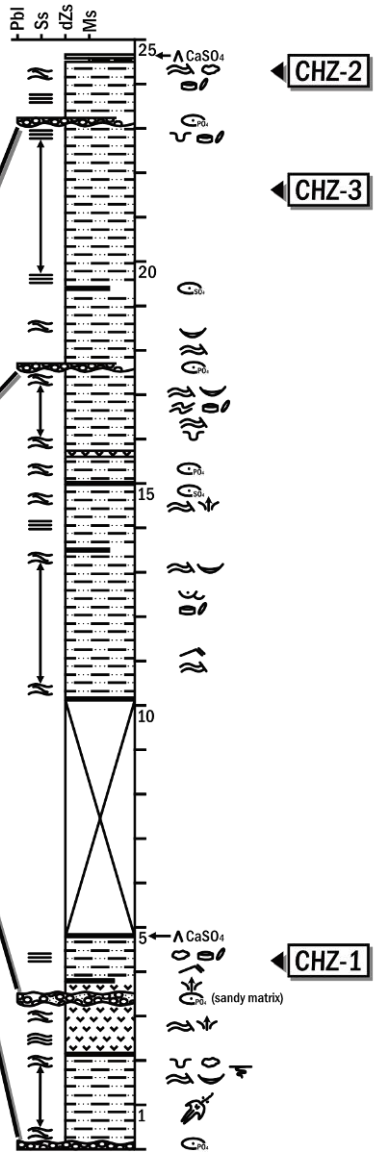

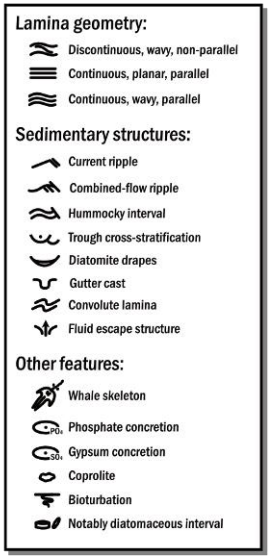

Cerro Hueco la Zorra / CHZ-1 / -14.46458,-75.70053

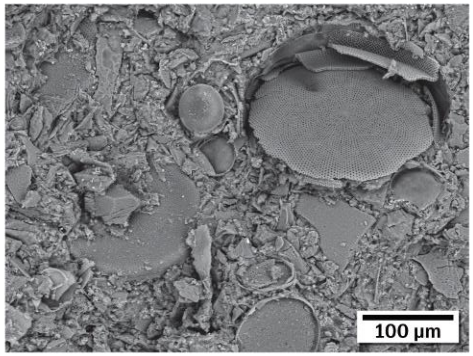

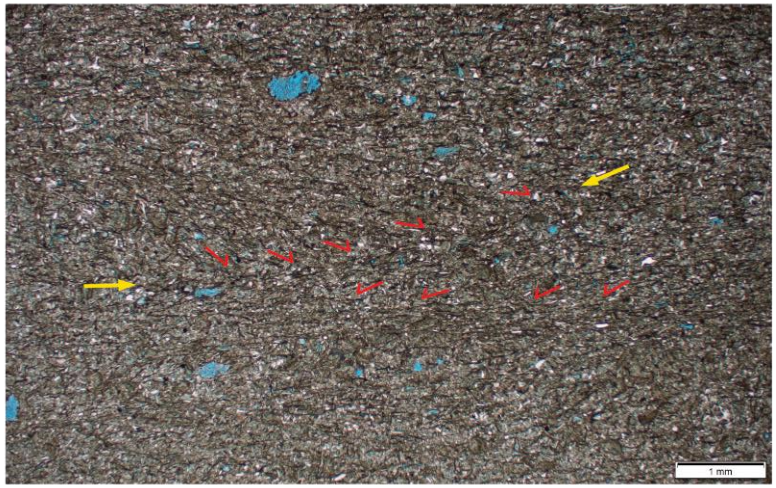

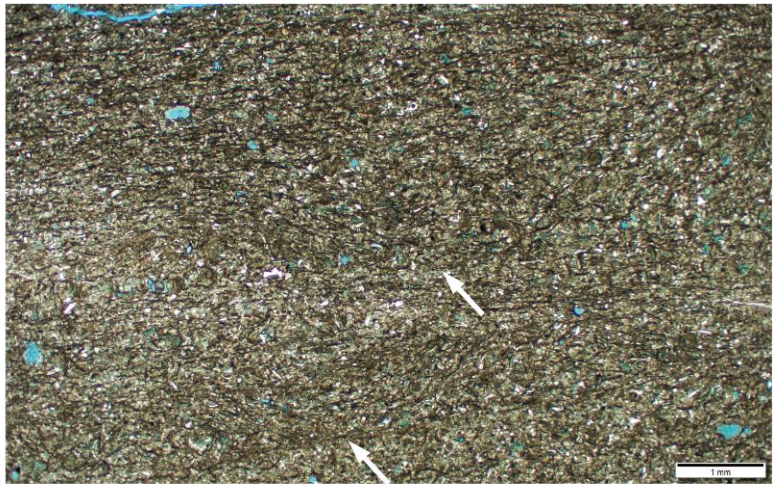

Outcrop description: Bright white with some orange staining at base; evaporate veins vertically cross-cut

Texture: Micro-cross-laminated diatomite

Lamina geometry: Largely wavy, discontinuous, and non-parallel; parallel at ripple foresets

Physical sedimentary structures: Troughs to swales (white arrows at bases), dipping foresets (red arrows), trucated surfaces (between yellow arrows), condensed centric-dominated internals

Other: Diatoms and platy grains conform to micro-laminae geometry

Interpretation: See Ch 2 for full description. Downlapping foresets suggest current ripple migration. Curved to wavy micro-laminae either represent current migration transverse to the field of view or wave ripples (there are some plausible signs of onlap in images presented in Ch 2).

Cerro Hueco la Zorra / CHZ-2 / -14.46458,-75.70053

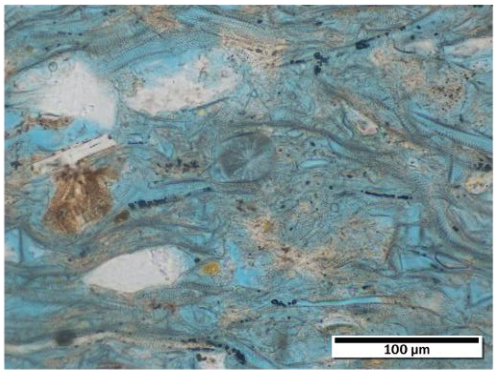

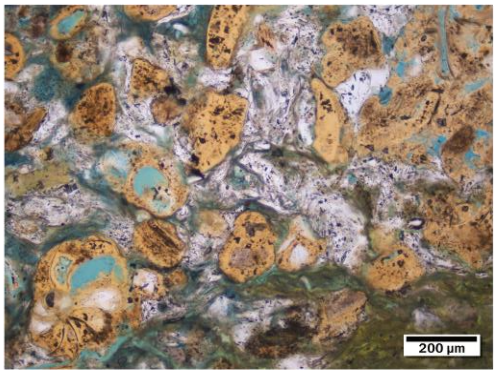

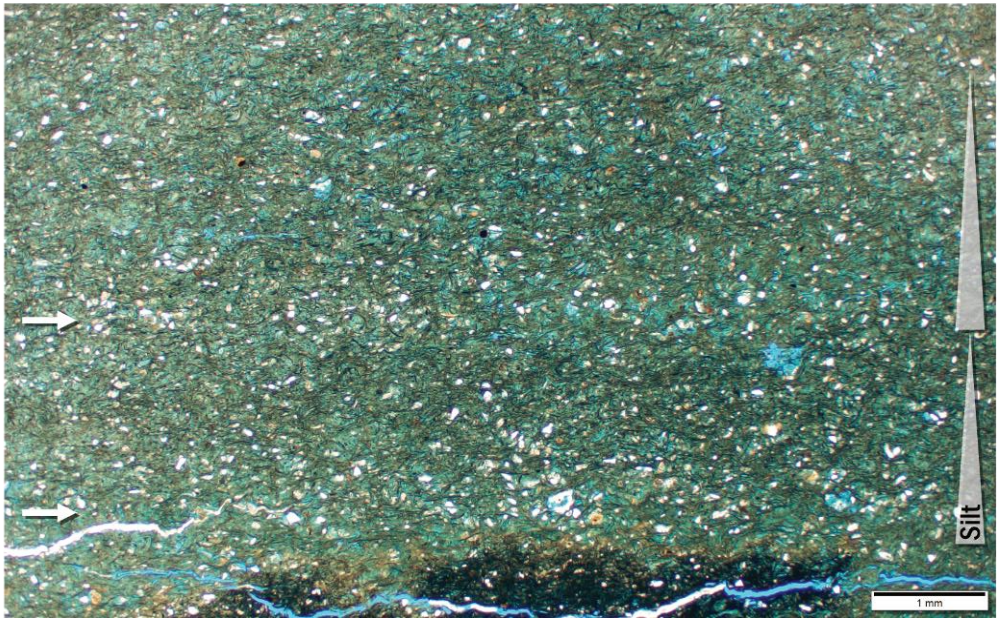

Outcrop description: Moderately fissile silty shale, white with mild yellow-orange staining on some laminae. Dark, overlying resistant bed is gypsum.

Texture: Silty diatomite

Lamina geometry: Indistinct in thin section, but appears planar, parallel, and continuous in outcrop

Physical sedimentary structures: Plausible silt laminae (along white arrows), plausible grading

Other: Higher amount of phosphate than in other samples (note phosphotized coprolite in Ch 2), coprolites

Interpretation: While largely diluted by high diatom content, plausible silt laminae and normal grading can be discerned in sample, suggesting a tractional genesis through floccule ripple migration. If so, continuity of laminae suggest transverse ripple migration under high sediment supply composed of mostly diatoms.

Cerro Hueco la Zorra / CHZ-3 / -14.46419,-75.70044

Outcrop description: Off-white and yellowish, some darker surface staining; evaporite veins vertically cross-cut

Texture: Diatomaceous siltstone, interlaminated

Lamina geometry: Parallel, continuous; varying from curved and wavy to planar. Planar lamination is truncated by curved laminae above (yellow arrow)

Physical sedimentary structures: Silt laminae (white arrows), normally graded laminae

Other: Diatoms appear to be mostly hash

Interpretation: The normally graded laminae suggests a possible genesis through silt-rich ripple migration. The continuous geometry of laminae further suggests high sediment supply and sedimentation rate, produced by transverse ripple migration (Yawar and Schieber, 2017). The silt-rich composition of the sample may have ground down the diatom component to hash during transport.

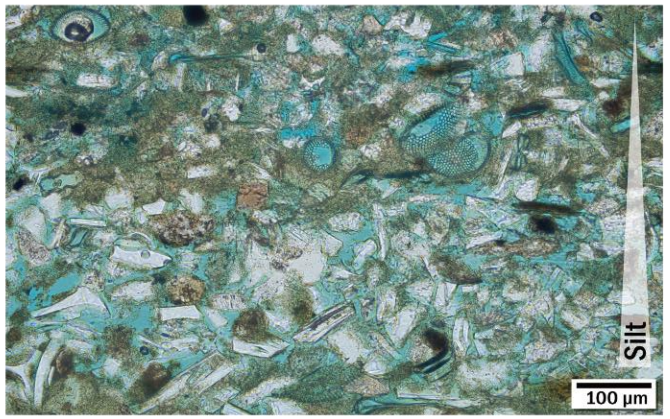

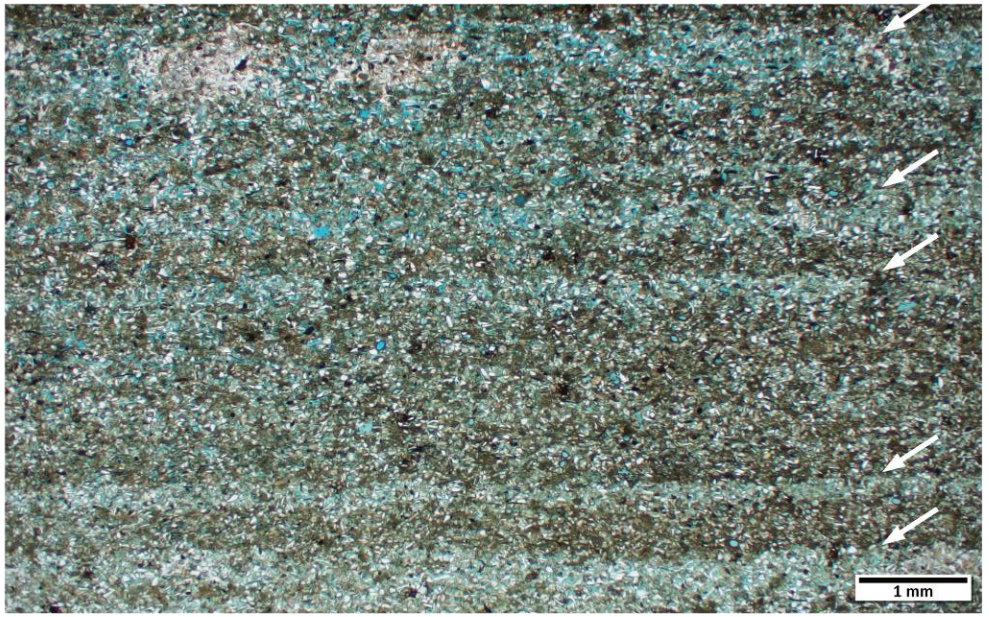

Cerro Pileta / CP-1 / -14.44502,-75.57530

Outcrop description: Extracted from a bright white tongue (yellow arrow) that stood out in outcrop even against the already light deposits of Cerro Pileta

Texture: Diatomite

Lamina geometry: Indistinct internal to tongue

Physical sedimentary structures: Possible silt lamina (white arrow, bottom right image)

Other: Appears centric dominated (200 µm diameter individuals, likely of the genera *Coscinodiscus*); contains an abundance of interstitial pennates as well, often in bundles as possible mat fragments (black circle, top left image)

Interpretation: Seem Ch2 for more description. With only one, diffuse silt lamina present, a tractional genesis for this sample remains dubious. However, due to the tongue's appear in outcrop and its near-purity in diatom content, this may represent an incredibly large diatom floccule. This is supported by the more random arrangement for centrics in the sample as well as the frequency of pennate bundles, known mat components. The sample was hosted in otherwise hummocky-swaley cross-stratified diatomite to diatomaceous siltstone, so it remains possible that the floccule was transported as one cohesive unit before deposition.

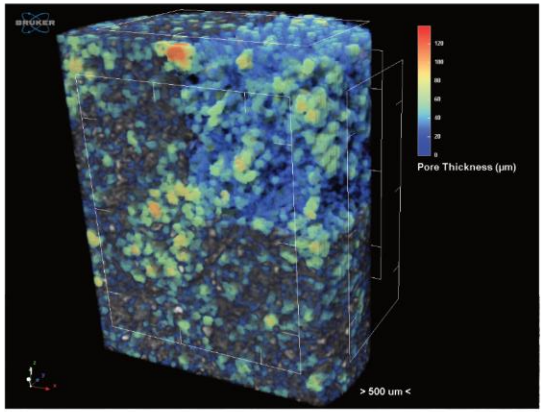

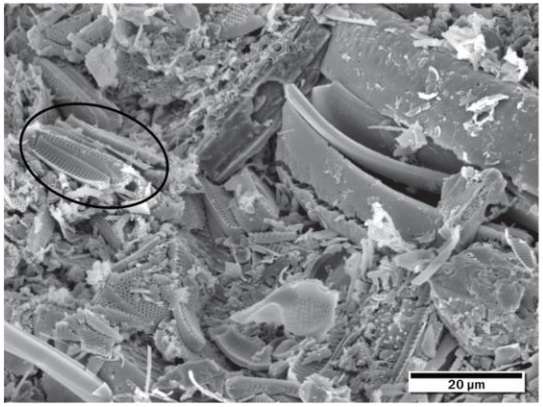

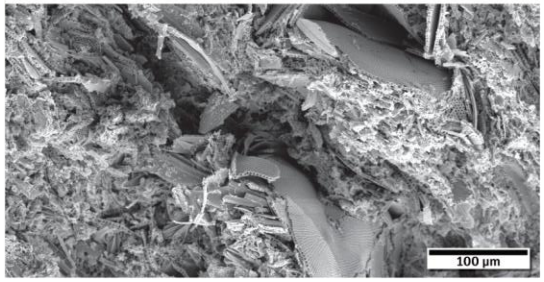

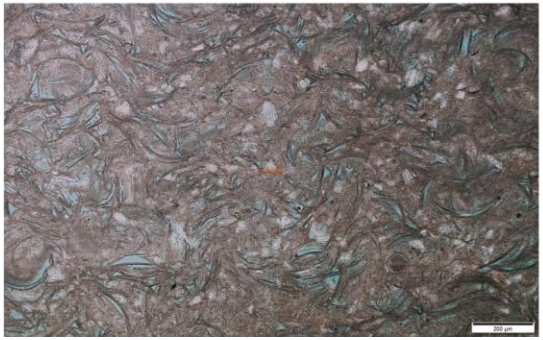

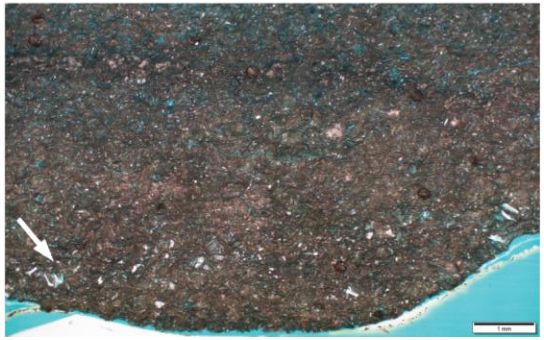

Cerro Pileta / CP-2 / -14.44510,-75.57570

Outcrop description: Off-white and yellowish, clearly cross-stratified

Texture: Silty diatomite

Lamina geometry: Curved to wavy, discontinuous, non-parallel

Physical sedimentary structures: Hummocky-swaley cross-stratified (in outcrop), coarse silt lenses (white arrows), normally graded

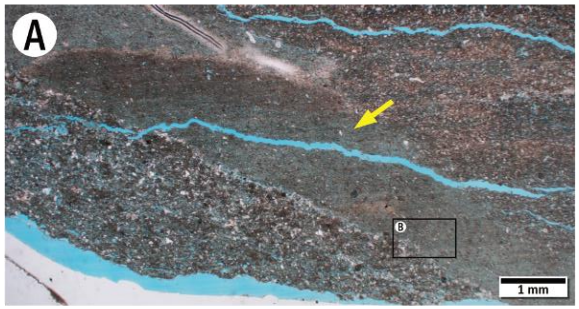

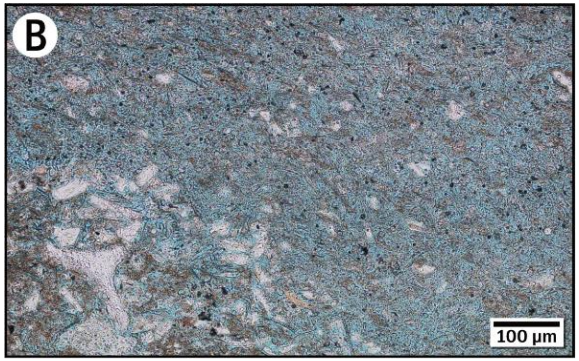

Other: Thin section went through some harsh processes, so cracks and ground-through intervals are not uncommon. Sample is also heavily artificially cracked as a result. During processing, a bright white tongue was spotted on sample, later revealed to be a dense mat or floccule of diatoms (yellow arrow), though exact composition is difficult to discern as the primary species appears to be a very narrow and fine pennate.

Interpretation: Besides outcrop stratification, thin section textures point to a tractional genesis for the sample by way of several, discontinuous lenses of coarser silt. This suggests a barchanoid style of floccule ripple migration (Yawar et al., 2017) possibly molded into hummocky-swaley cross-stratification during combined flow (see Ch 2 for further explanation.

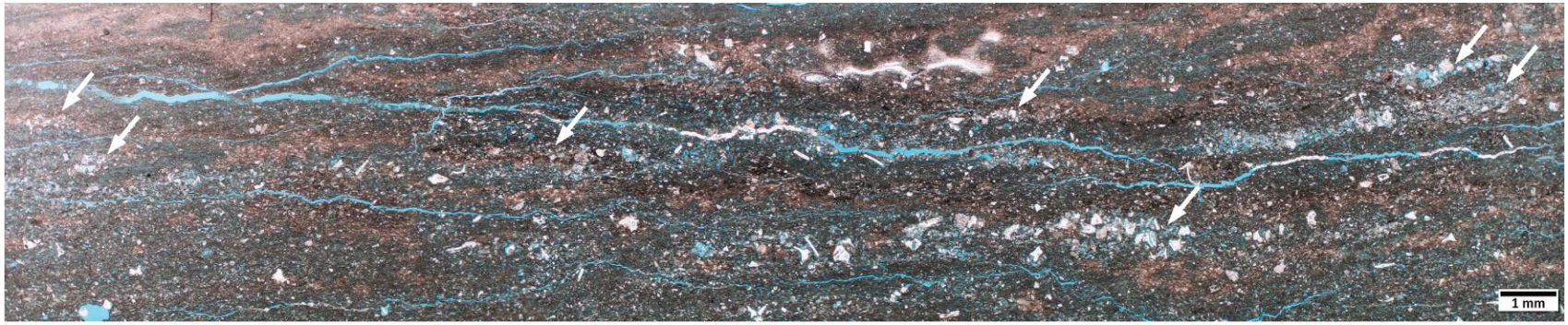

Cerro Pileta / CP-3 / -14.43188,-75.57672

Outcrop description: White swale draping with some marginal soft-sediment deformation

Texture: Silty diatomite

Lamina geometry: Curved to planar, continuous, parallel

Physical sedimentary structures: Coarser silt laminae (white arrows) overlain by bedded to laminated diatomite hosting finer silt; normally graded laminae and beds

Other: Coarse silt appears to more readily exhume than the surrounding, finer substrate (in contrast to other mudstones where clay is usually most readily weathered over coarser material). *Chaetoceros* resting spores were also observed in SEM (yellow arrow).

Interpretation: Presence of continuous and successive silt laminae suggest deposition as a result of transverse floccule ripple migration (Yawar et al., 2017). Variances in lamina and bed size may reflect a variance of sediment concentration within the hyperpycnal-like sediment gravity flows which successively filled in the scoured swale seen in outcrop (see Ch 2 for full process description).

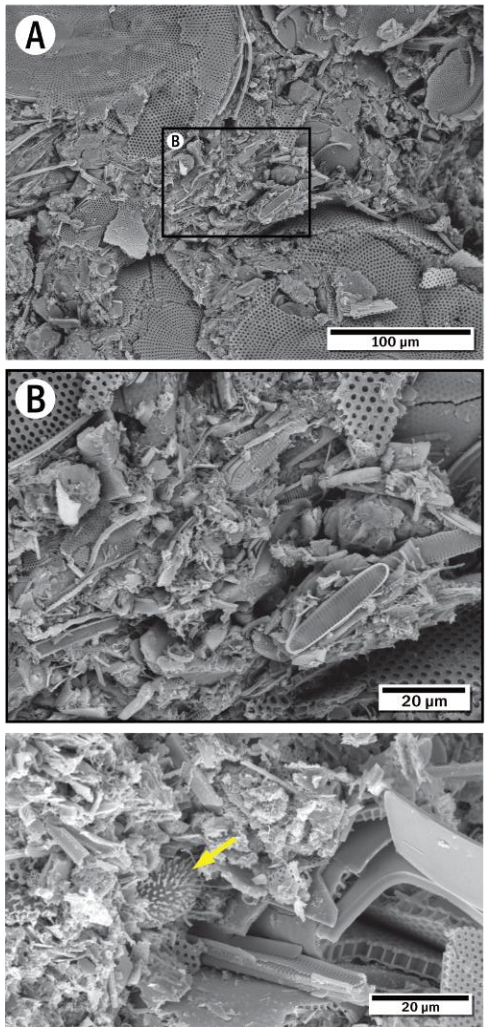

Cerro Pileta / CP-4 / -14.44483,-75.57536

Outcrop description: White, hummocky-swaley cross-stratified, visibly coarser than most diatomite; sample extracted near fluid escape trace (yellow box)

Texture: Silty diatomite

Lamina geometry: Wavy to curved, discontinuous, non-parallel

Physical sedimentary structures: Coarser silt laminae, normally graded, gentle truncation

Other: Larger mat fragments of pennates were observed (white arrow). Silt component of sample is largely vesicular ash and contains more biotite than other samples.

Interpretation: See Ch 2 for full description. Presence of continuous silt laminae suggest deposition as a result of transverse floccule ripple migration (Yawar et al., 2017) or hyperpyncal-like sediment gravity flows. Gentle truncation is likely a result of combined flow which molded migrating sediment into hummocky-swaley bedforms. Fluid escape likely occurred soon after deposition.

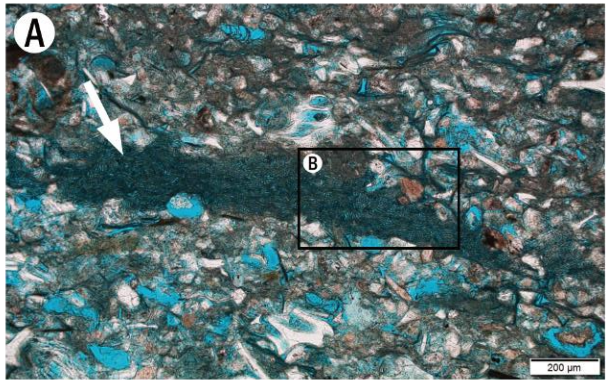

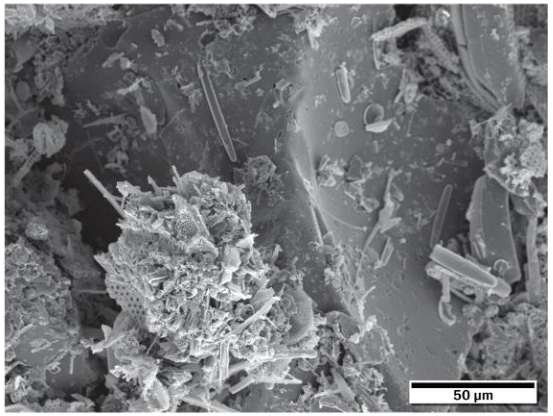

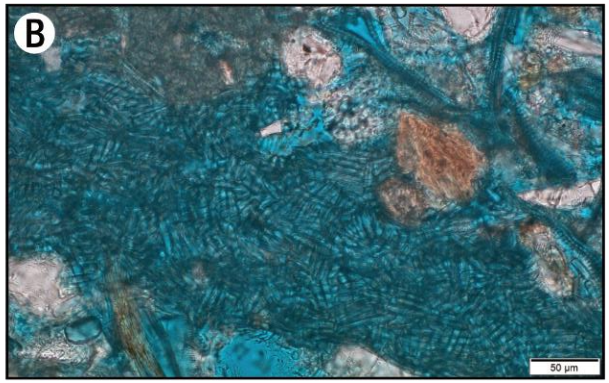

Cerro Mamá y la Hija / CMZ-1 / -14.61005,-75.67671

Outcrop description: Channel drape containing internal, interlaminated siltstone-diatomite

Texture: Diatomaceous siltstone with some diatomite laminations

Lamina geometry: Continuous and planar to wavy, non-parallel and discontinuous

Physical sedimentary structures:
Graded couplets of siltstone capped in diatomite (some showing better grading than others). One is interpreted as the product of a wave enhanced sediment-graivty flow or WESGFs (see Ch 2)

Other: Larger diatoms occur in caps of couplets (yellow arrow). Smaller diatoms can occur in the coarse silt component of couplets (white arrow). Thus, the silt component is normally graded while the diatom component is reverse graded.

Interpretation: See Ch 2 for full description. Channel is interpreted as the product of storm scour successively filled by hyperpycnal-like sediment gravity flows, some entrained by storm waves in high enough concentrations to form WESGFs. Flows form couplets normally graded in silt and reverse graded in diatoms (note arrows). Stratification becomes more wavy as channel fills and flows are exposed to overriding currents. Top is bioturbated due to post-storm colonization of infauna.